Finite element modelling: Analysis of Reinforced Concrete Elements

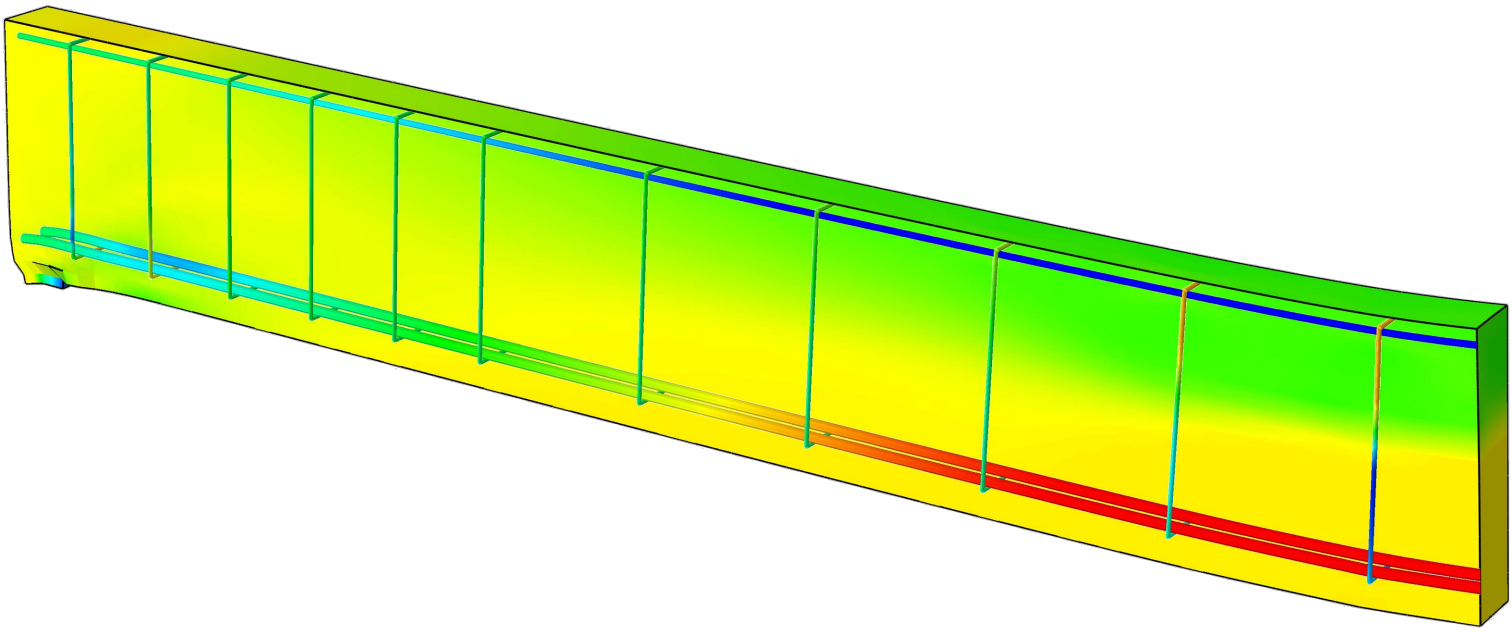

Laurentiu-Fabian Bitiusca
M.Sc. in Structural and Civil Engineering
Master's Thesis
July 13th 2016

AALBORG UNIVERSITY
STUDENT REPORT

AALBORG UNIVERSITY
STUDENT REPORT

The School of Engineering and Science
Study Board of Civil Engineering
Fibigerstræde 10, 9220 Aalborg Ø
http://www.ses.aau.dk/

Title

Finite Element Modelling:
Analysis of Reinforced Concrete Elements

Type of thesis

Master's Thesis

Project period

March 2016 - July 2016

Student

Laurentiu-Fabian Bitiusca

Supervisors

Johan Clausen

Synopsis:

This project contains analytic and finite element calculations of a reinforced concrete member. The report identifies and verifies different cross-sections for serviceability and ultimate limit states. Steel bars are placed in relevant regions inside the concrete mass and as a result both flexural and shear effects upon the beam are considered during calculations.
From the analytic calculations it is concluded that the involved reinforced concrete section which is based on the formulae accounting for shear reinforcement return the safest design in the end.
Based on the strength class, of both concrete and steel materials, and also on the corresponding deformation parameters non-linear analyses are performed using a finite element commercial software.
Different stress-strain based material behaviour models are investigated. It is concluded that for a first estimate the use of Mohr-Coulomb model is deemed acceptable if fine touches are done to tune the model for concrete. For a proper analysis however the Concrete Damage Plasticity model is the best solution as the obtained results agree more to those analytically computed and furthermore if the necessary parameters are available crack patterns can also be shown.

Printed copies: 3
Report pages: 62
Appendix pages: 10
Completed July 13th 2016

Preface

This report is written as a part of the Master's programme in Structural and Civil Engineering at Aalborg University and represents the final thesis. *Finite Element Modelling: Analysis of Reinforced Concrete Elements* is the topic of the project.

Prerequisites for reading the report is basic knowledge regarding civil engineering and reinforced concrete structures.

Great gratitude is addressed to the supervisor of the project, Assoc. prof. Johan Clausen for guidance, constructive criticism and inspiring supervision during the project.

Reading guide
References to available sources are in the format of Harvard method, and a complete source list is stated in the bibliography. In the project, references are made for sources with either "[Surname/Organisation, Year]" or "Surname/Organisation [Year]" and, when relevant, specific pages, tables or figures may be asserted. Websites are specified by author, title, URL and date. Books are mentioned by author, title, publisher and edition, as long as it is available. Papers are furthermore cited with journal, conference papers with time and venue, when available.

The report includes figures and tables, which are enumerated according to their respective chapter. E.g. the first figure in chapter 5 appears with number 5.1, the second number 5.2 and so on.

In the report references are made to folders on the enclosure-CD which contains digital enclosures of various kinds. The reference format match with, "[Enclosures-CD, Folder name]".

Laurentiu-Fabian Bitiusca

Table of contents

Introduction 1

In this chapter, the project subjects and goals are presented and selected analyses are listed and motivated.

1.1 Project relevance

Structures made out of concrete material in combination with steel bars, which is used as reinforcement, are designed in large proportions even in the modern days, with the tallest building in the world, as visible in Figure 1.1, emphasising this idea.

Figure 1.1. Burj Khalifa during construction stage [Moghrabi, 2006].

The result of the mixture between concrete and steel is widely used for structural elements such as beams, columns, slabs, walls etc. Thus, reinforced concrete members can be subjected to loads of higher magnitudes, acting simultaneously on different directions and of distinct types, from static to dynamic loads, with the latter presenting stress reversals. As a consequence, in order to achieve such remarkable structures and to be able to perform a good design, first and foremost an understanding of the involved materials is essential.

From all of the mentioned structural elements, the reinforced concrete beam (see Figure 1.2) subjected to external loads can show the behaviour of the material to some extent as such a member is possible to undergo compressive, tensile and shear stresses all at once. Along these lines, a simply supported beam having a uniformly distributed load on top is the main topic which is chosen to be discussed in the project.

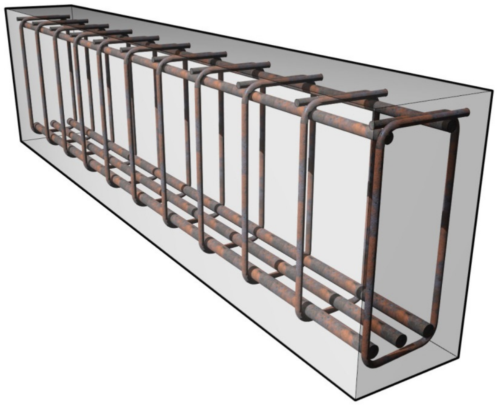

Figure 1.2. Reinforced concrete beam representation [Vasshaug, 2013].

1.2 Problem statement

Common design analytic procedures for reinforced concrete beams imply different assumptions on the actual behaviour of the materials, with constant stresses, along the height of the section, in most cases being applied. Even tough it is stated that the derived equations do account for plastic effects, the problem becomes more uncertain in case of non-linear cases.

In the following paragraphs, the treated problem fields and the imposed objectives for the current project are described. Thus, the considered and investigated questions with respect to a reinforced concrete beam section are:

- With the proposed beam geometry and characteristics an investigation is performed for both serviceability and ultimate limit states. Certain analytic methods and design formulae are applied. What are the involved assumptions and by how much do these influence the results?
- Beams can come in different sizes, both in cross-section and in length, while different boundary conditions can also be accounted for, thus as a consequence failure can occur due to a number of reasons. What is the main failure mechanism of the involved beam?
- Reinforcement can be attributed to specific regions inside of the beam member to strengthen it. For the investigated case do these different types add safety in terms of bearing capacity?
- Due to the highly non-linear response of concrete, finite element commercial software are considered. How large difference is obtained from the existent analytic methods and do the obtained results agree to a certain extent?

The report seeks verification of the reinforced concrete beam and as a result the formulae are used for this specific scope only, as furthermore they can also be applied for a conceptual design.

Hardening and softening laws for the concrete behaviour in both tension and compression are available in the literature and it is desirable to implement such laws in the computations carried with the aid of an appropiate commercial software.

Different material constitutive models are available for finite element calculations. Hence, some of the most relevant ones and which could probably return reliable results for the present case are chosen and investigated.

Materials 2

In this chapter the materials involved in the analysis are presented and the behaviour of both plain concrete and steel reinforcement is explained. For calculations see [Enclosures-CD, Chapter 2].

2.1 Plain concrete

Concrete is one of the most widely used structural materials. The main reasons that reinforces this statement are described briefly as follows:

- Economical aspect: the leading factor which always portrays a new construction is its cost. As a comparison, a concrete structure can be half the price of a steel one.
- Variety: concrete can be used in order to achieve a wide diversity of shapes and dimensions, that will return a pleasant structural and architectural construction.
- Fire resistance: structures made of concrete have a resistance of up to three hours without requiring any special measures as opposed to steel structures.
- Availability: the main components sand, cement and gravel are easily found in the most locations.
- Maintenance: constructions made of concrete are easier to maintain than steel structures, thus leading to a reduction in costs.

However, as any other material, concrete also has some disadvantages. Among these its necessity of being supported by formwork while construction, high unit weight, low resistance to weight ratio and tensile strength (0.1 - 0.2 of the compressive strength) stand out. While the first one will always be present, the other issues can be addressed either by choosing a lightweight aggregate in its composition, a high resistance class or by associating concrete with steel. Thus, with respect to the last situation, the well known reinforced concrete material is obtained.

2.1.1 Concrete behaviour

As all materials, concrete is deformable. Nonetheless, its behaviour is complex and can not be represented well through the currently available idealized models visible in Figure 2.1 a) and b). Under loading, the stress-strain relation is highly non-linear and unsymmetrical. Moreover, residual deformations are present when unloading takes places. This behaviours can be represented as shown in Figure 2.1 c).

So, the material is best defined by its increased performance in compression when loaded. Thus, structures subjected primarily to compression behave very well and can resist very high forces. Still, as stated in Section 2.1, while subjected to tensile forces concrete by itself can represent a major threat if used alone.

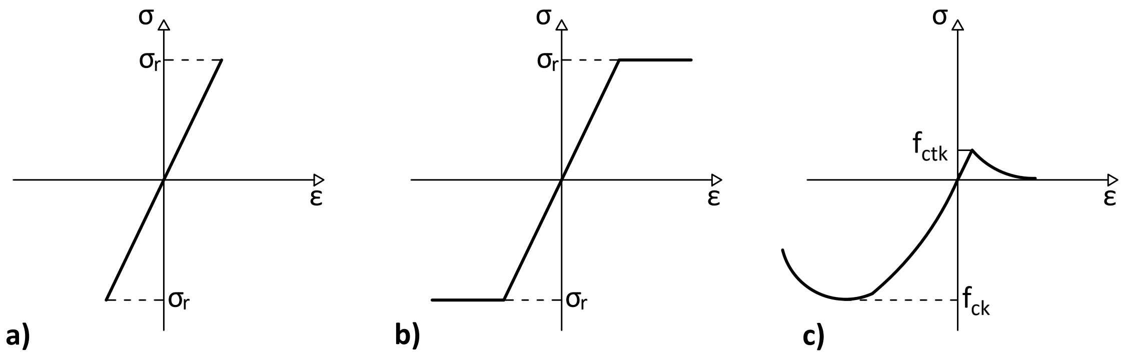

Figure 2.1. Stress-strain relations for: a) Linear-elastic material b) Linear elastic-perfectly plastic material and c) Plain concrete [Pascu, 2008].

Material properties

In order to represent the stress-strain relationship used in both analytical calculations and finite element (FE) analysis, the material properties must be chosen. Usually the compressive strength of concrete is given as strength classes that relate to the characteristic 5% cylinder strength, f_{ck}. For the present project a concrete of class C 20/25 is chosen. This means the material during testing of a specimen in compression exhibited a cylinder strength of 20 MPa and cube strength of 25 MPa. With respect to this class the material characteristics are afterwards computed as specified in EN1992-1-1 [2014].

To represent the behaviour of concrete in tension, the tensile strength is firstly found by the use of Equation (2.1).

$$f_{ctk,0.05} = 0.7 f_{ctm} \tag{2.1}$$

where

$f_{ctk,0.05}$	Tensile strength of concrete found as 5%-fractile
f_{ctm}	Mean tensile strength of concrete, $f_{ctm} = 2.12 \ln\left(1 + \left(\frac{f_{cm}}{10}\right)\right)$

For certain stages, like demoulding or transfer of prestress, is required to define the compressive strength at a young age, usually up to 28 days, as indicated in Equation (2.2). According to EN1992-1-1 [2014] it is a good assumption to rewrite this relation in order to obtain the actual mean compression strength of concrete. The considered values are taken from Table 3.1 which can be found in the Eurocode.

$$f_{ck}(t) = f_{cm}(t) - 8\,\text{MPa} \quad , \quad 3 \leq t \leq 28 \tag{2.2}$$

$$f_{cm} = f_{ck} + 8\,\text{MPa} \tag{2.3}$$

where

f_{cm}	Mean compression strength of concrete, $f_{cm} = 31\,\text{MPa}$
f_{ck}	Compressive strength of concrete, $f_{ck} = 25\,\text{MPa}$

The calculated value of tensile strength equals 2.16 MPa. Another important characteristic of the concrete behaviour curve is the modulus of elasticity. As concrete is made of a mixture of materials, the elastic deformations depend mostly on the material composition, so it is in return controlled by the moduli of elasticity of its components. The considered secant modulus is found by Equation (2.4) indicated in EN1992-1-1 [2014]. However, its value might change if concrete presents a big amount of limestone and sandstone and can be reduced from 10% to 30%. Regardless, for general applications EN1992-1-1 [2014] stated this as a good approximate.

$$E_{cm} = \left(22\left(\frac{f_{cm}}{10}\right)^{0.3}\right)10^3 \tag{2.4}$$

The calculated value represented in Figure 2.2 a) is found to be 3.15×10^4 MPa and is taken at an approximation of $0.4f_{cm}$.

Stress-strain relationship

A conventional stress-strain relationship for concrete subjected to uniaxial compression was proposed by Hognestad [1951] and is calculated by Equation (2.5). The curve, which is shown in Figure 2.2 b), assumes a non-linear variation from the the beginning of loading which might not be entirely true as concrete can have a linear elastic response in its early state. After reaching the peak value concrete starts to softens and this behaviour is represented by a linear variation prior to failing by crushing at an ultimate strain.

$$\begin{aligned} \frac{\sigma}{f_{ck}} &= 2\frac{\varepsilon}{\varepsilon_{c2}}\left(1-\frac{\varepsilon}{2\varepsilon_{c2}}\right) \quad , \quad 0<\varepsilon<\varepsilon_{c2} \\ \frac{\sigma}{f_{ck}} &= 1-0.15\left(\frac{\varepsilon-\varepsilon_{c2}}{\varepsilon_{cu2}-\varepsilon_{c2}}\right) \quad , \quad \varepsilon_{c2}<\varepsilon<\varepsilon_{cu2} \end{aligned} \tag{2.5}$$

where

σ	Stress
ε	Strain
ε_{c2}	Strain at reaching the maximum strength, $\varepsilon_{c2} = 0.002$
ε_{cu2}	Ultimate strain, $\varepsilon_{cu2} = 0.0035$

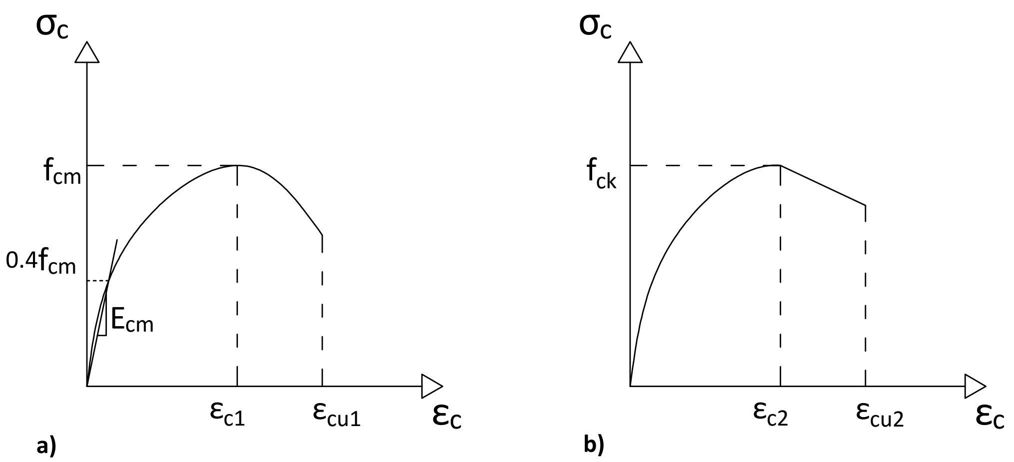

Figure 2.2. Representation of a) Secant modulus b) Stress-strain relationship [Hognestad, 1951].

For the sole purpose of the design of a beam cross-section the same relation as recommended by Hognestad [1951] for the hardening part is also specified by the Eurocode. Thus, all analytic calculations in the project are based on this assumption.

As in compression, concrete in tension is highly non-linear. In order to represent as good as possible this behaviour Bruno Massicotte and MacGregor [1990] assumed a linear-elastic brittle material with strain softening. Thus, he suggested a post-cracking stress-strain relationship for the tensile part of the curve which was latter modified in order to allow for a gradual response. This behaviour can be seen in Figure 2.3 where the assumed strain relations at different stresses can also be noticed.

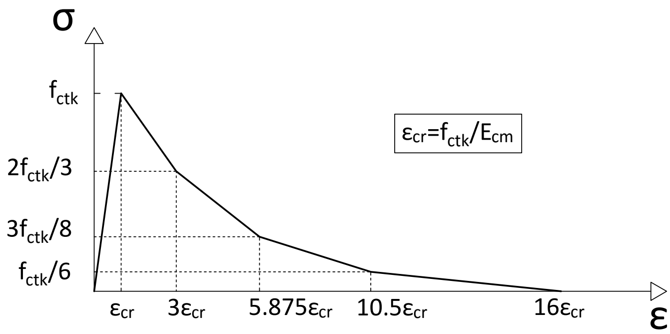

Figure 2.3. Modified [Bruno Massicotte and MacGregor, 1990] tension softening curve.

In order to capture the real life situation of the material, two stress-strain curves for the concrete behaviour have been proposed and they are visible in Figure 2.4.

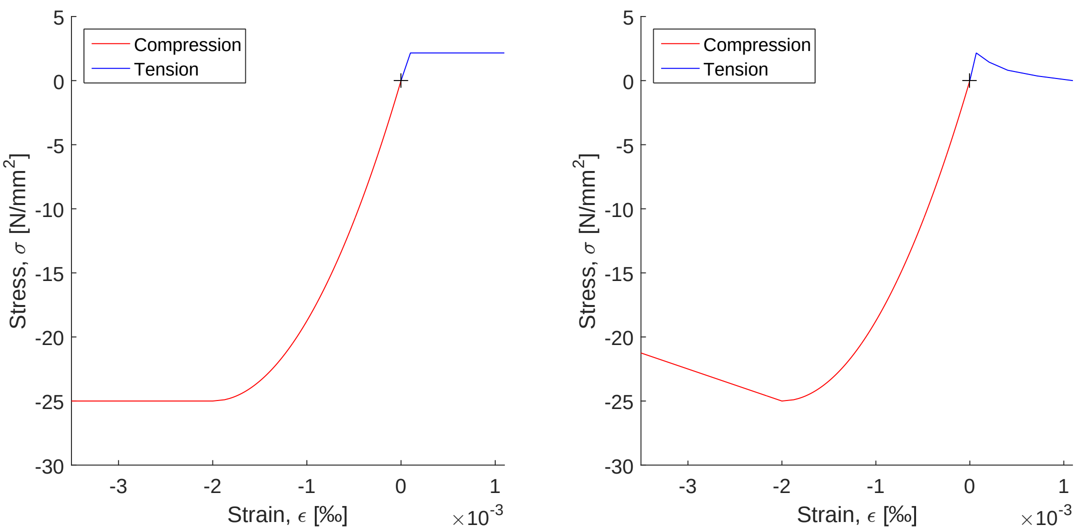

Figure 2.4. Stress-strain relationship a) Calculated by EN1992-1-1 [2014] b) Proposed by [Hognestad, 1951] and [Bruno Massicotte and MacGregor, 1990].

Both curves are considered in a first simulation for the numerical calculations and the one which give the best outcome is used to obtain the output results.

2.2 Steel

Steel composition is mainly consisting of iron and carbon. So, if the quantity of carbon is high then the resistance increases but it becomes more prone to corrosion. Moreover, the resistance to fire is low and in return special and expensive treatments must be applied to secure the structural integrity. These are one of the major drawbacks in constructing structures made solely of steel. However, steel used as reinforcement for structural elements has a low quantity of carbon (usually bellow 0.4%) and is fire protected by the concrete material.

2.2.1 Steel behaviour

It is well known that steel is a material which behaves very good when subjected to tensile stresses, while concrete does not. Thus, this is the primary reason of the association between concrete and steel. For ensuring a favourable steel behaviour under serviceability limit state (SLS) loads it must be mentioned that actually what is important is the elastic limit of steel and not its resistance at rupture. This limit vary depending on the mark of steel between 240 MPa and 600 MPa.

The rebars used as reinforcing material are obtained in two different ways. They can either be hot-rolled or cold-worked and with respect to the involved process they behave differently.

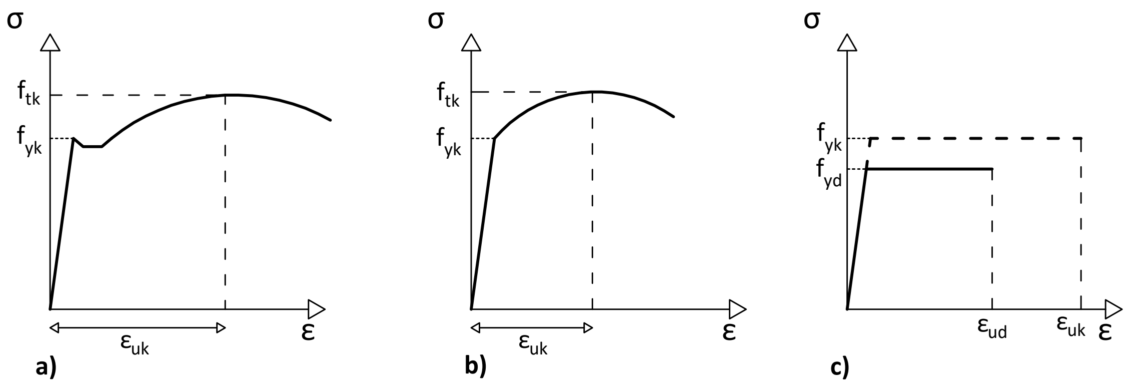

Figure 2.5. Stress-strain diagrams of reinforcing steel: a) Hot-rolled b) Cold-worked and c) Idealized behaviour for steel in both tension and compression [Pascu, 2008].

For the first type illustrated by Figure 2.5 a) rebars with distinct yielding plateau and good ductility are obtained. Ductility represent the post-elastic deformation capacity without losing the strength and is an important characteristic for reinforced concrete elements. The steel bars obtained by cold-working do not show the plateau and usually their deformation capacity is lower.

As shown in Figure 2.5 c) for the current project an idealized linear-elastic perfectly-plastic behaviour for the steel bars is considered according to EN1992-1-1 [2014]. Moreover, steel of class S345 has been selected and this has a yielding strength of 345 MPa, while the modulus of elasticity has been chosen to be equal to 2.1×10^5 MPa.

Part I

Reinforced concrete beam

Analytic approach 3

This chapter provides a complete analysis for a reinforced concrete beam. First the properties of the beam are presented. Afterwards two different cross-sections are considered and their results are discussed. Moreover, the shear resistance is checked and corresponding reinforcement is provided. Calculations can be found on [Enclosures-CD, Chapter 3].

3.1 Beam characteristics

The geometric and material parameters are chosen respecting the design regulations and limitations imposed by the Eurocode. Thus, it is assumed that the analysed beam represents reality and is feasible from the construction point of view. The general properties of the proposed reinforced concrete beam are given in Table 3.1 and its corresponding geometry is visible in Figure 3.1. Moreover the material characteristics for both concrete and steel are specified in Chapter 2.

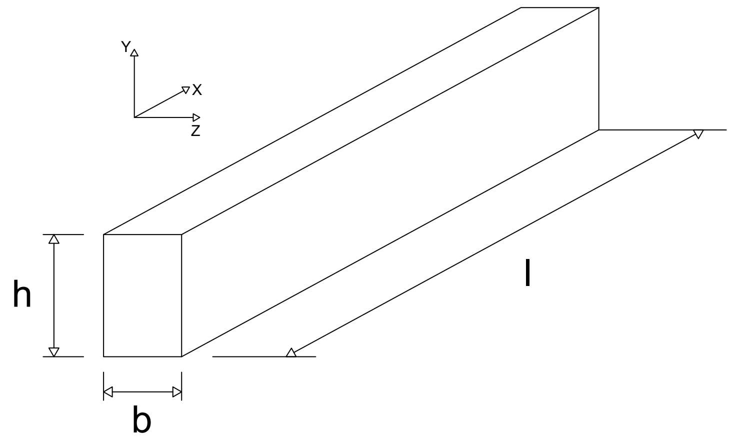

Figure 3.1. Considered beam geometry.

Table 3.1. General beam properties.

Length, l [m]	Width, b [m]	Height, h [m]
10	0.25	0.50

3.1.1 Euler-Bernoulli beam theory

For a SLS analysis the classical beam theory is used in order to obtain the displacements. For the current project this is assumed for linear elasticity only which means Hooke's Law must be respected. For an appropriate analytic computation procedure certain assumptions are established and listed bellow and they are the base for the classical beam theory approach.

- Weightless beam: the self weight of the beam is not taken into account.
- Plane symmetry: straight longitudinal axis and in any point along it the corresponding cross-section has a plane of symmetry.
- Cross-section: constant or with small variation.
- Material model: the involved material is elastic and isotropic, while non-homogeneous material such as reinforced concrete is also considered.
- Perpendicularity: plane sections remain plane and normal to the deformed longitudinal axis during and after bending takes place.
- Linearity: rotations and deformations are slightly changing such that the conditions of infinitesimal theory is applicable.
- Strain energy: the energy stored during deformations is due to bending moment, while the shear and axial forces are neglected.

Static scheme and boundary conditions

The beam visible in Figure 3.2 a) is considered to be simply-supported and subject to an uniform load. With respect to this case the corresponding deflection can be calculated using Bernoulli theory.

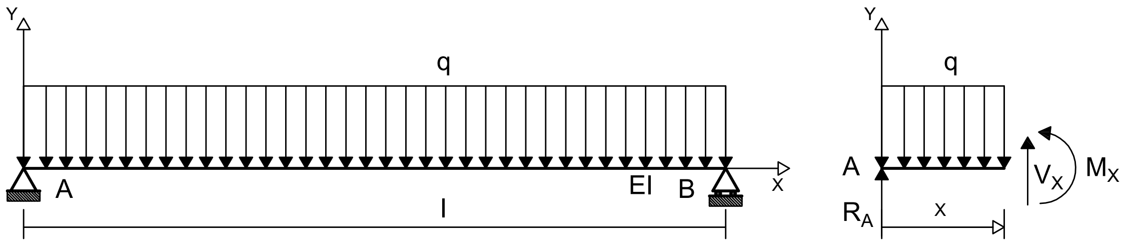

Figure 3.2. Boundary conditions of the imposed beam.

First, the moment equilibrium equation is written with respect to point x in Figure 3.2 b). In this way, Equation (3.1) returns the bending moment about the considered point.

$$M_X = R_A x - \frac{qx^2}{2} \tag{3.1}$$

where

q	uniform distributed load
R_A	reaction at point A, $R_A = \dfrac{ql}{2}$

As stated in the strain energy assumption Bernoulli linked the internal energy to the stresses and strains from bending only. Thus, the resultant bending moment is written in the form:

$$M_z(x) = -EI\frac{d^2\delta}{dx^2} \tag{3.2}$$

where

EI	flexural rigidity
δ	beam deflection

By equalling Equation (3.1) to Equation (3.2) and afterwards integrating twice, Equation (3.3) is obtained. Moreover, by applying the characteristic kinematic boundary conditions for a simply-supported beam at points A and B the expression for the deflection at mid-point is given by Equation (3.4).

$$EI\delta = \frac{qx^3}{24}(2l - x) + C_1 x + C_2 \tag{3.3}$$

$$\delta_{mid} = -\frac{5ql^4}{384EI} \tag{3.4}$$

where

C_1	first integral constant, $C_1 = -\dfrac{ql^3}{24}$
C_2	second intergral constant, $C_2 = 0$

The minus sign in Equation (3.4) is only an indication that the displacement points downwards. This means that for further calculations the absolute value is going to be considered.

3.2 Singly reinforced beam

For a first analysis involving longitudinal steel bars, particular material parameters must be established beforehand. Thus, following the guidelines imposed by EN1992-1-1 [2014] , Table 3.2 present the specifications of both concrete and steel. Moreover, Figure 3.3 a) illustrate the chosen reinforced beam cross-section.

Table 3.2. Material parameters.

Concrete				Steel	
f_{ck}	25 MPa	η	1.0	f_{yk}	345 MPa
E_{cm}	3.15×10^4 MPa	λ	0.8	E_s	2.1×10^5 MPa
a	30 mm			ϕ	20 mm
ε_{cu2}	0.0035			ε_y	0.0016

The ultimate limit state (ULS) deformation for concrete, ε_{cu2}, and yielding deformation for steel, ε_y, are provided by EN1992-1-1 [2014]. Coefficients η and λ represent the effective strength factor and effective height of the compressed zone respectively. They are chosen with respect to the concrete compressive strength. Moreover, the concrete cover, represented by the parameter a, is chosen following the regulations such that both fire protection and steel erosion is prevented.

The tensile strength of concrete is neglected in hand calculations due to the fact that it has little contribution and most of the tensile stress is carried over by the longitudinal bars in tension.

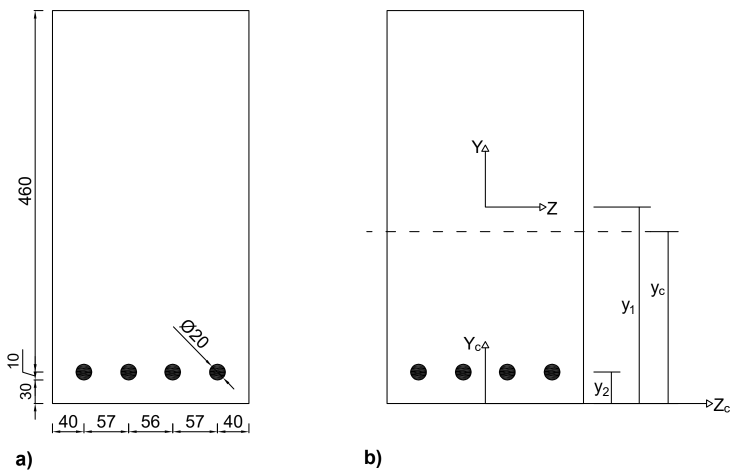

Figure 3.3. a) Cross-section of a singly-reinforced concrete beam b) Centroid of the section.

3.2.1 Flexural rigidity

Since the cross-section in discussion represents a heterogeneous material, the flexural rigidity must be found. Considering a new system of coordinates at the bottom part of the section (see Figure 3.3 b)), by using Equation (3.5) the center of mass is found. Moreover, the stiffness moduli is different and the centroid is calculated with respect to this criterion.

$$y_c = \frac{\sum A_i y_i E_i}{\sum A_i E_i} \Rightarrow y_c = \frac{A_{cs} y_1 E_{cm} - n_h A_h y_2 (E_{cm} - E_s)}{A_{cs} E_{cm} - n_h A_h (E_{cm} - E_s)} \tag{3.5}$$

where

A_{cs}	rectangular cross-section area, $A_{cs} = bh$
A_h	area of the holes, $A_h = \frac{\pi \phi^2}{4}$
n_h	number of holes
y_1, y_2	distance from the bottom fibre to the center of each shape
ϕ	bar diameter

The corresponding moment of inertia for the rectangular concrete cross-section with holes is found by solving Equation (3.6). Afterwards, the flexural rigidity for the heterogeneous reinforced concrete beam is computed using Equation (3.7). Thus, due to the value of steel modulus of elasticity a stiffer behaviour for the beam is going to be achieved.

$$I_c = I_{cs} + A_{cs} (y_1 - y_c)^2 - n_h \left(I_h + A_h (y_2 - y_c)^2 \right) \tag{3.6}$$

$$EI = E_{cm} I_c + n_h E_s \left(I_h + A_h (y_2 - y_c)^2 \right) \tag{3.7}$$

where

I_c	moment of inertia of cross-section with holes
I_{cs}	moment of inertia of rectangular cross-section, $I_{cs} = \frac{bh^3}{12}$
I_h	moment of inertia of circular hole, $I_h = \frac{\pi \left(\frac{\phi}{2}\right)^4}{4}$

Displacement

For the SLS analysis a load is chosen such that it is assumed the reinforced concrete beam is still in its early stage of service and under linear-elastic behaviour. The displacement at the mid-span is introduced already in Section 3.1.1 with the Equation (3.4). Thus, q_{SLS} is substituted and the allowed displacement according to the analytical calculations is afterwards found. The results for the SLS case are found in Table 3.3.

Table 3.3. Analytic results for SLS.

$q_{SLS}\left[\frac{\text{KN}}{\text{m}}\right]$	δ [mm]
15.00	2.77

3.2.2 Stress-strain distribution

The concept of balanced design shown in Figure 3.4 a) is applied when investigating reinforced concrete cross-section. This comes from similarity of triangles and states that if both ε_s and ε_c, at their corresponding stresses, are reached at the same time then a balanced failure condition must exists and this is calculated by means of Equation (3.8).

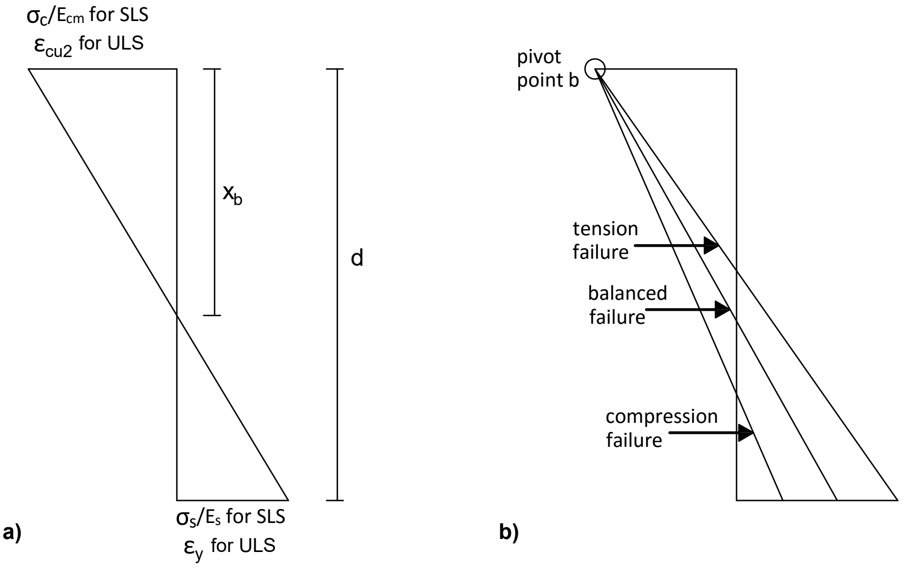

Figure 3.4. Strain diagrams for concrete a) For balanced failure b) Comparative strain diagrams

$$\frac{x_b}{d-x_b} = \frac{\varepsilon_c}{\varepsilon_s} \Rightarrow x_b = d\frac{\varepsilon_c}{\varepsilon_c+\varepsilon_s} \tag{3.8}$$

where

ε_c	strain at top fibre
ε_s	strain in steel bar
x_b	the critical height
d	design height of the cross-section

The most economical reinforced concrete section in terms of materials usage is by considering that maximum stresses in reinforcement and concrete reach their ultimate values at the same time. Thus, the best possible way to design a cross-section is by using the critical height, x_b, as the height of compressed part. However, most of the time this can not be done as the area of steel does not satisfy the imposed condition due to the current available bar diameters. So, it is imposed that the value of the compressed height, x, to be smaller than the critical one, which means is better to use an amount of steel (or a steel class) in the beam less than that at a balance failure (see Figure 3.4 b)). By doing so, the actual stress in steel reaches the yield strength, f_{yk}, but is still capable of sustaining loads as steel is a ductile material. In contrast, the stress in concrete is less than the compressive strength, f_{ck}. This is known as an under-reinforced section and in this case failure is gradual.

Over-reinforced sections contain more reinforcement than needed and are dominated by the compression failure of concrete. In this case an increased load develops over stress in concrete prior to the reinforcement and as a consequence concrete crushes in compression. This type of failure occurs suddenly and is mandatory to be avoided. Therefore, for safety and economic reasons, flexural members must be designed as under-reinforced sections.

ULS

For a singly-reinforced beam with the longitudinal steel bars placed in the tension zone the ultimate state approach is specified by EN1992-1-1 [2014] and is shown in Figure 3.5. This proposal takes into account plasticity of concrete under loading. Moreover it allows for a simplified analytic calculation because a non-linear distribution of the stresses is easier solved by a numerical software. Hence, it is an assumption to the real behaviour indicated by the curved line in the same illustration.

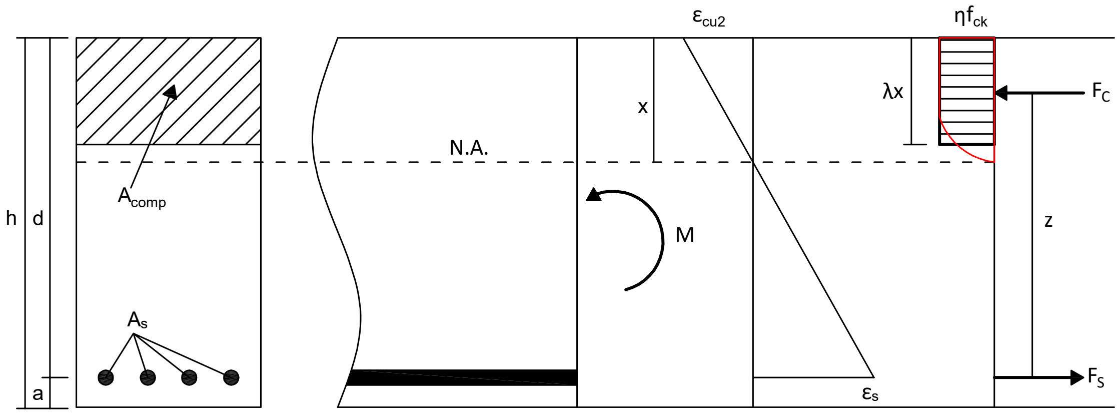

Figure 3.5. Rectangular stress distribution.

One must be pointed out that reinforcement should yield before the appearance of the first crack in concrete and concrete must fail before failure of the steel bars. This assumption is treated with the aid of Equation (3.9) which relates the strains of both steel and concrete. The same concept of balanced design as for the SLS is imposed here but now the strains are considered at their ultimate values.

$$x_b = d\varepsilon_b \quad with \quad \varepsilon_b = \frac{\varepsilon_{cu2}}{\varepsilon_{cu2} + \varepsilon_y} \tag{3.9}$$

In order to find the moment capacity, M_{cap}, of the structural element, the height of the compressed area must be determined first and also this must agree with the criteria specified earlier.

Considering the method of equilibrium of a section given by Equation (3.10), x can be in return computed by Equation (3.11). If the condition is not met the stress of the steel bars is lower than f_{yk} and the bars are not utilised at their full capacity. It is thus economically feasible to use the value of x_b instead or to select a lower steel class.

$$F_C = F_S \Leftrightarrow \lambda x \eta f_{ck} b = n_h A_s f_{yk} \tag{3.10}$$

$$\begin{aligned} x &= \frac{n_h A_s f_{yk}}{\lambda \eta f_{ck} b} \quad , \quad x \leq x_b \\ x &= x_b \quad , \quad x > x_b \end{aligned} \tag{3.11}$$

where

F_C	forces on the compressive side
F_S	forces on the tensile side
A_s	area of steel bar cross-section

To check the condition imposed by Equation (3.9) in terms of strains, x_b is substituted by the newly found x and ε_y is calculated as ε_s. By checking the value of ε_s in Table 3.4 against ε_y is concluded that the criteria is fulfilled and steel bars reach yielding prior to failure of concrete.

The moment capacity of the reinforced concrete beam is found by computing the moment from either the steel reinforcement or from the concrete area in compression. These two relations are shown in Equation (3.12). However, if the yielding criteria is not met a lower steel class should be selected or as an alternative Equation (3.13) could be used for calculating M_{cap}.

$$M_{cap} = n_h A_s f_{yk} z \quad or \quad M_{cap} = b\lambda x \eta f_{ck} z \quad , \quad x \leq x_b \tag{3.12}$$

$$M_{cap} = b\lambda x_b f_{ck} z \quad , \quad x > x_b \tag{3.13}$$

where

z	the arm of the force, $z = d - \dfrac{\lambda x}{2}$

As for the SLS case, the bending moment can be calculated at the mid-span of the beam using the moment equilibrium principle. Thus, the solution of Equation (3.14) is the bearing capacity after imposing the value of M_{cap}.

$$M_{mid} = \frac{ql^2}{8} \Rightarrow q_{cap} = \frac{8M_{cap}}{l^2} \tag{3.14}$$

where

q_{cap}	bearing capacity of the beam

Table 3.4. Analytic results for ULS.

M_{cap} [KNm]	$q_{cap}\left[\frac{\text{KN}}{\text{m}}\right]$	δ [mm]	ε_s [-]	ε_c [-]	x [mm]
184.40	41.00	-	0.0151	0.0035	86.71

3.3 Doubly reinforced beam

There are mainly three reasons why steel reinforcement is used in the compressed area:

- due to architectural design or aesthetics the dimensions of the cross-sections are limited; mainly the height. Thus, the loads acting on the beam surpass the moment capacity of a singly reinforced one.
- when a combination of forces give a moment of opposite sign on the cross-section.
- reinforcement at the top part can act as a formwork for the stirrups while it can also increase the lifetime of the structural element as it behaves better to long-time deformations.

The same material parameters given in Table 3.2 are utilised here with the addition that for the compressed longitudinal bars the diameter is chosen to be equal to 12 mm and the yielding strength to 235 MPa. In Figure 3.6 a) the chosen reinforced beam cross-section is visible.

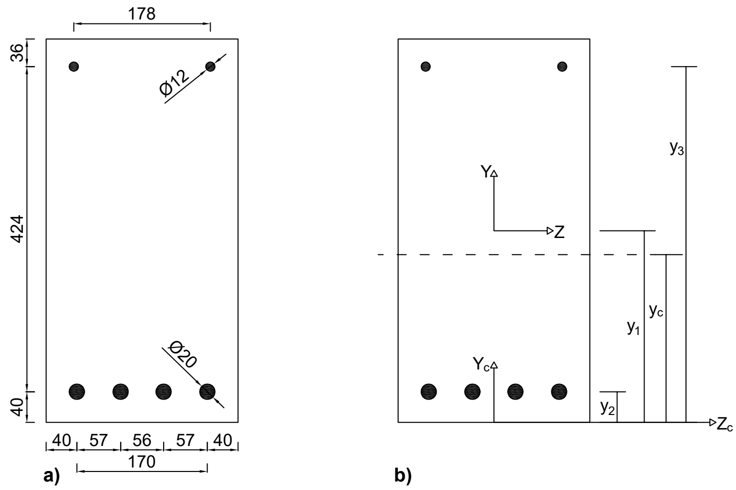

Figure 3.6. a) Cross-section of the doubly-reinforced concrete beam b) Centroid of the section.

3.3.1 Flexural rigidity

The same procedure as for the singly reinforced cross-section beam is carried out for the new involved case. Hence, the center of mass is calculated by means of Equation (3.15) and as illustrated in Figure 3.6 b).

$$y_c = \frac{A_{cs}y_1E_{cm} - (n_{h1}A_{h1}y_2 + n_{h2}A_{h2}y_3)(E_{cm} - E_s)}{A_{cs}E_{cm} - (n_{h1}A_{h1} + n_{h2}A_{h2})(E_{cm} - E_s)} \tag{3.15}$$

where

A_{h1}	area of the holes for bars in tension, $A_{h1} = \dfrac{\pi\phi_1^2}{4}$
A_{h2}	area of the holes for bars in compression, $A_{h2} = \dfrac{\pi\phi_2^2}{4}$
n_{h1}, n_{h2}	number of holes for their corresponding steel bars
y_3	distance from the bottom fibre to the center of its corresponding shape
ϕ_1, ϕ_2	bar diameters in tensile and compressive part respectively

The moment of inertia for concrete is calculated with Equation (3.16) and subsequently the flexural rigidity is computed using Equation (3.17). As the effect of steel is introduced in a larger area and steel has a good behaviour under tensile stresses, the beam should be more stiff than the one which has a section with bottom bars only.

$$I_c = I_{cs} + A_{cs}\,(y_1 - y_c)^2 - \left(n_{h1}\left(I_{h1} + A_{h1}\,(y_2 - y_c)^2\right) + n_{h2}\left(I_{h2} + A_{h2}\,(y_3 - y_c)^2\right)\right) \tag{3.16}$$

$$EI = E_{cm}I_c + n_{h1}E_s\left(I_{h1} + A_{h1}\,(y_2 - y_c)^2\right) + n_{h2}E_s\left(I_{h2} + A_{h2}\,(y_3 - y_c)^2\right) \tag{3.17}$$

where

I_c	moment of inertia of cross-section with holes
I_{h1}	moment of inertia of bottom circular hole, $I_{h1} = \dfrac{\pi\left(\frac{\phi_1}{2}\right)^4}{4}$
I_{h2}	moment of inertia of top circular hole, $I_{h2} = \dfrac{\pi\left(\frac{\phi_2}{2}\right)^4}{4}$

Displacement

The same load, q_{SLS}, as considered for the singly-reinforced beam is kept and afterwards, the displacement is found with the aid of Equation (3.4) given by Bernoulli's beam theory. The results for a concrete beam reinforced with both compressed and tensioned bars are visible in Table 3.5.

Table 3.5. Analytic results for SLS.

$q_{SLS}\left[\frac{\mathrm{KN}}{\mathrm{m}}\right]$	δ [mm]
15.00	2.71

3.3.2 Stress-strain distribution

The concept of balanced design demonstrated for a cross-section with longitudinal bars placed only in the tensioned zone (see Figure 3.4) holds true also for the doubly-reinforced concrete beam. Thus, in order for the steel bars to reach yielding the same condition must be satisfied.

ULS

In the case of a beam with both top and bottom longitudinal reinforcement the stress-strain distribution diagrams change depending on the state of strain in the compressed steel [EN1992-

1-1, 2014]. This behaviour can be seen in Figure 3.7 and it follows that the moment capacity is calculated by means of either case a) or b).

With respect to either of the two involved cases presented in Figure 3.7 the diagram of stress distribution changes accordingly and the corresponding forces that act on the cross-section are shown in Figure 3.8.

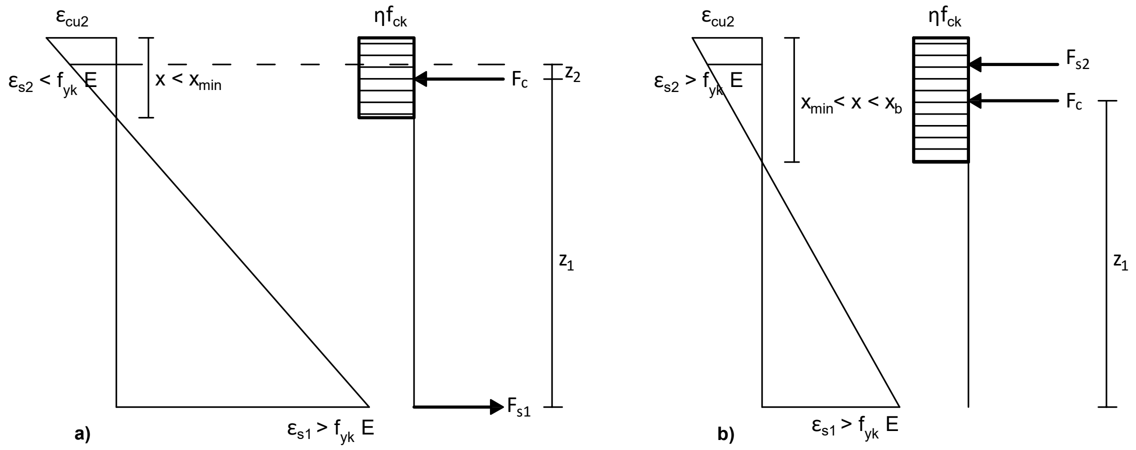

Figure 3.7. Strain and stress diagrams for a cross-section with compressed reinforcement.

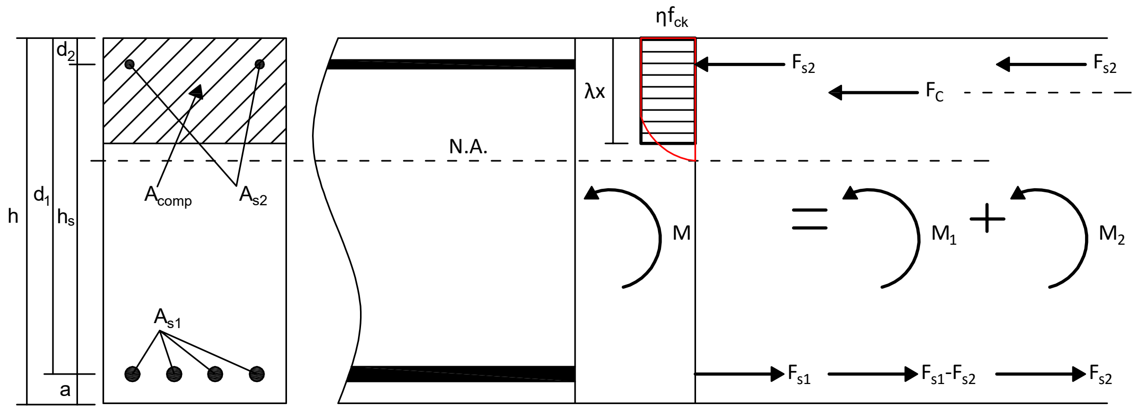

Figure 3.8. Rectangular stress distribution.

The same yield criteria as pointed out in Section 3.2.2 for ULS case must be satisfied here also. However it is not necessarily for the steel bars in the compressed zone to reach yielding, but only for the tensile side. If this is the case then a singly-reinforced cross-section beam will be capable of sustaining the external loads just about as much as the doubly-reinforced one.

The condition for the tensioned bars to reach yielding is imposed by Equation (3.18) while for the compressed bars Equation (3.19) comes into play.

$$\varepsilon_{s1} > \varepsilon_y \Rightarrow x_b = d_1 \frac{\varepsilon_{cu2}}{\varepsilon_{cu2} + \varepsilon_y} \quad , \quad x \leq x_b \tag{3.18}$$

$$\varepsilon_{s2} > \varepsilon_y \Rightarrow x_{min} = d_2 \frac{\varepsilon_{cu2}}{\varepsilon_{cu2} - \varepsilon_y} \quad , \quad x_{min} < x \tag{3.19}$$

where

x_{min}	minimum height of the compressed area
ε_{s1}	strain of the tensioned bars
ε_{s2}	strain of the compressed bars
d_1, d_2	design heights of the cross-section corresponding to case a) and b)

To calculate the moment capacity of the structural element the height of the compressed area must be determined first. Considering the method of equilibrium of a section given by Equation (3.20), this height can be in return computed by Equation (3.21). If the imposed condition for the bars placed in the tension is not met it is preferably to either chose another steel class with a lower value for f_{yk} or imposing x_b as the height of compressed area.

$$F_C = F_S \Leftrightarrow \lambda x \eta f_{ck} b = n_{h1} A_{s1} f_{yk} - n_{h2} A_{s2} f_{yk} \tag{3.20}$$

$$x = \frac{n_{h1} A_{s1} f_{yk} - n_{h2} A_{s2} f_{yk}}{\lambda \eta f_{ck} b} \quad , \quad x \leq x_b \tag{3.21}$$

where

F_C	forces on the compressive side
F_S	forces on the tensile side

Results

In order to find the strains in the top and bottom fibres, ε_{s1} and ε_{s2}, Equation (3.18) and Equation (3.18) are rearranged so that the known quantity is the previously calculated x. Afterwards, following the corresponding case, M_{cap} is computed using Equation (3.22) or Equation (3.23). It must be however pointed out that in the second case a beam with longitudinal bars placed only on the bottom part is better from the economical point of view.

$$M_{cap} = b\lambda x \eta f_{ck} z_1 + n_{h2} A_{s2} f_{yk} h_s \quad , \quad x_{min} \leq x \leq x_b \tag{3.22}$$

$$M_{cap} = b\lambda x \eta f_{ck} z_2 + n_{h1} A_{s1} f_{yk} h_s \quad , \quad x < x_{min} \tag{3.23}$$

where

z_1	downward-arm of the resultant force F_c, $z_1 = d_1 - \dfrac{\lambda x}{2}$
z_2	upward-arm of the resultant force F_c, $z_2 = d_2 - \dfrac{\lambda x}{2}$
h_s	distance between tensioned and compressed bars, $h_s = h - (d_1 + d_2)$

The same principle as denoted by Equation (3.14) for the singly-reinforced section is applied in order to obtain the bearing capacity. The displacement is not of interest at ULS and the most important parameter is the value of q_{cap}. The characteristic analytic results for a doubly-reinforced concrete beam can be found in Table 3.6.

Table 3.6. Analytic results at ULS.

M_{cap} [KNm]	q_{cap} $\left[\frac{\text{KN}}{\text{m}}\right]$	δ [mm]	ε_{s1} [-]	ε_{s2} [-]	ε_c	x [mm]
186.51	41.45	-	0.0191	0.0017	0.0035	71.10

3.4 Effect of shear force

For a simply-supported beam the shear force is represented as shown in Figure 3.9 a). Thus, as the magnitude of it increases the angle α between the horizontal and the direction of the principal stresses increases as well (see Figure 3.9 b)). This means that in the regions close to the supports the principal stresses become more and more inclined. This has the effect that in the specified areas cracks are also forming with an inclination as they follow the direction of the compressive stresses.

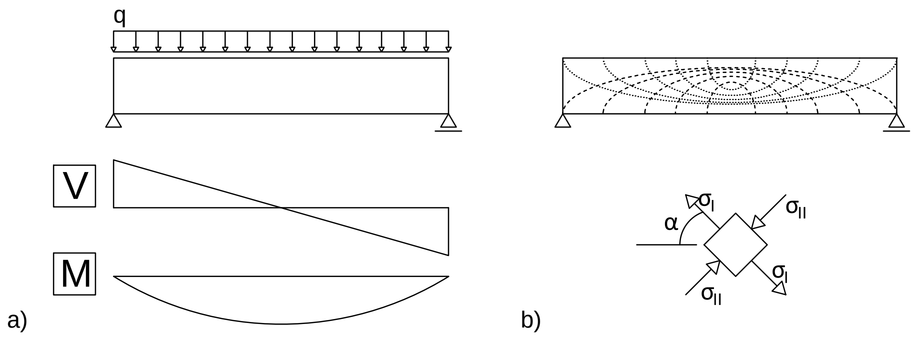

Figure 3.9. a) Static scheme simply-supported beam b) Principal stresses direction and influence of the shear upon them [Pascu, 2008].

Moreover, the application of shear force creates a biaxial state of stress in concrete, mainly compression and tension. In order for concrete to sustain shear it is required that $\sigma_I \leq f_{ctk}$ and $\sigma_{II} \leq f_{ck}$, with σ_I and σ_{II} being principal stresses. If the stress in tension is greater than the actual tensile strength of concrete than the section must be reinforced with steel bars for shear, while if the second condition is not satisfied the concrete section must be enlarged [Pascu, 2008].

In order to check if such reinforcement is required, EN1992-1-1 [2014] (under Section 6.2.2) states that first it must be checked if the design shear resistance of the member without shear reinforcement, $V_{Rd,c}$, withstand the actual force. This is calculated based on Equation (3.24) and must satisfy the imposed condition.

$$\begin{aligned} V_{Rd,c} &= \left[0.12k\left(100\frac{A_{sl}}{b_w d}f_{ck}\right)^{\frac{1}{3}}\right]b_w d \quad , \quad V_{Ed} \leq V_{Rd,c} \\ k &= 1+\sqrt{\frac{200}{d}} \end{aligned} \tag{3.24}$$

where

A_{sl}	area of the tensile reinforcement, $A_{sl} = A_{s1}$
b_w	smallest width of the cross-section in the tensile area, $b_w = b$
V_{Ed}	shear force at support in the doubly reinforced section, $V_{Ed} = \dfrac{q_{cap}l}{2}$
q_{cap}	bearing capacity given in Table 3.6

The assumption of using the shear force at the support obtained from the bearing capacity of the doubly reinforced section is rather crude, but since no design loads are given this was opted for. Thus, if the condition is not satisfied shear reinforcement is required and according to EN1992-1-1

[2014] this must be disposed on a specific distance close to the support as visible in Figure 3.10. The reason for this is explained further down when the actual shear resistance is calculated.

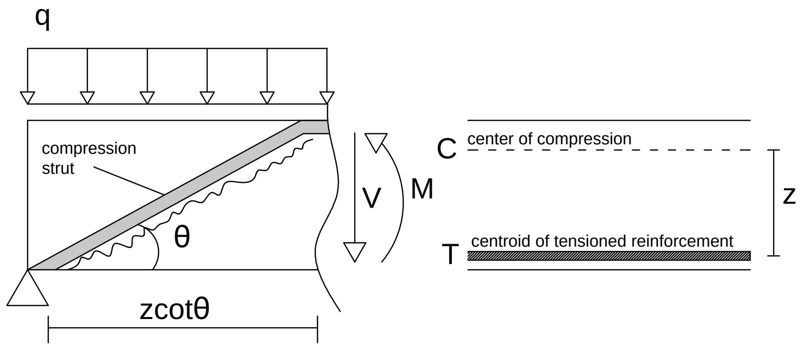

Figure 3.10. Span along which transverse reinforcement should be accounted for [Pascu, 2008].

In order to find the necessary reinforcement in the member the calculations are based on a truss model as shown in Figure 3.11, where the inclined dashed lines are the compression struts and the vertical full lines represent the stirrups. Hence, a beam with inclined cracks develops in the upper and lower fibres compressive and tensile forces, vertical tension in the stirrups and inclined compressive forces in the concrete "diagonals" between cracks. There are two types of reinforcement that accounts for shear, essentially vertical or inclined stirrups. In case of static loads, cf. Figure 3.9, the principal tensile stresses are much more inclined where shear forces are of importance, so an inclined reinforcement along the direction of these stresses is much more effective. However, for the case of seismic loads, due to the presence of stress reversals, the vertical reinforcement becomes much more effective as these reversals causes cracking parallel to the inclined bars [MacGregor and Wight, 2012]. In the present project no such loads are involved so both cases are considered for a direct comparison with the FE analysis results.

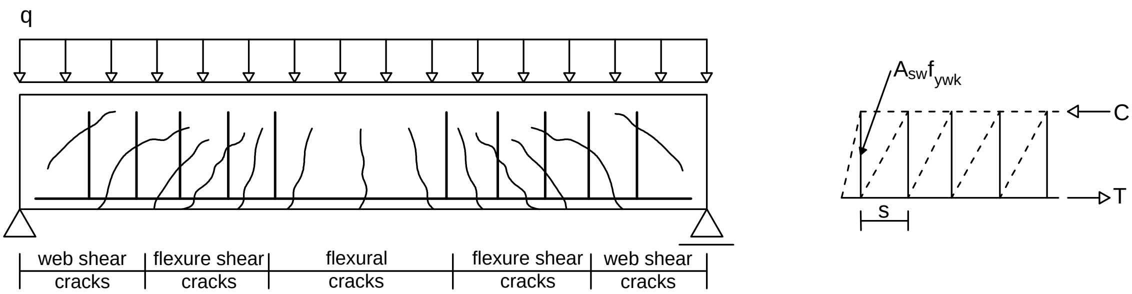

Figure 3.11. Plastic truss model [MacGregor and Wight, 2012].

3.4.1 Transverse rebars

Placing longitudinal steel bars in the compressed zone might add an extra safety measure during service of the structural element. However, their main purpose is to keep the stirrups in position. Thus, for members that are reinforced with vertical stirrups, the shear resistance, V_{Rd}, is calculated by means of Equation (3.25) from which the minimum value between the shear force sustained by the yielding shear reinforcement, $V_{Rd,s}$, and maximum shear force sustained by the member, $V_{Rd,max}$, is the considered one [EN1992-1-1, 2014].

$$\begin{aligned} V_{Rd,s} &= \frac{A_{sw}}{s} z f_{ywk} \cot\theta \\ V_{Rd,max} &= \alpha_{cw} b_w z \nu_1 f_{ck} \frac{1}{\cot\theta + \tan\theta} \\ \nu_1 &= 0.6\left(1 - \frac{f_{ck}}{250}\right) \end{aligned} \tag{3.25}$$

where

A_{sw}	cross-sectional area of the shear reinforcement, $A_{sw} = 2\frac{\pi\phi_s^2}{4}$
ϕ_s	diameter of the transverse stirrup as sketched in Figure 3.12
s	spacing of the stirrups
z	lever arm, $z = 0.9d$
f_{ywk}	characteristic yield strength of the shear reinforcement
θ	angle between the concrete compression strut and the horizontal axis, $21.8° \leq \theta \leq 45°$
α_{cw}	coefficient which accounts for the state of stress in the compression chord, $\alpha_{cw} = 1$
ν_1	strength reduction factor for concrete cracked in shear

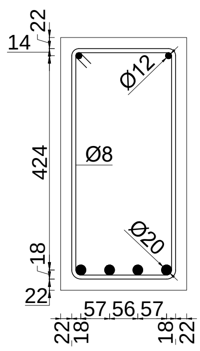

Figure 3.12. Section sketch.

For the current case the yield strength of the stirrups is chosen with respect to a steel class of S235 in order to comply with the yielding criterion. Moreover, EN1992-1-1 [2014] states that shear force has higher influence in the length equal to $z\cot\theta$ from the face of the support as seen in Figure 3.10 and as a result is better to place the stirrups denser in this region. So, in order to ensure a greater span along which the stirrups are placed much closely to each other, the angle θ is chosen as the lower limit. Afterwards the spacing between stirrups is taken with respect to the condition imposed by the Equation (3.26).

$$\frac{A_{sw}}{s} \geq \frac{V_{Ed}}{f_{ywk} z \cot\theta} \Rightarrow s \leq \frac{A_{sw} f_{ywk} z \cot\theta}{V_{Ed}} \tag{3.26}$$

The obtained results are given in Table 3.7, where it can be seen that an increased bearing capacity is achieved compared to the doubly reinforced section.

Table 3.7. Analytic results for transverse reinforcement.

V_{Rd} [KN]	q_{cap} $\left[\frac{\text{KN}}{\text{m}}\right]$	s mm
125.40	41.80	195

A sketch of how the stirrups are arranged is shown in Figure 3.13 and as discussed they are disposed much denser close to the ends, while towards the middle of the beam they are more wider placed. The difference between the doubly reinforced section with and without the stirrups is the leading factor in order to get an understanding of their effects.

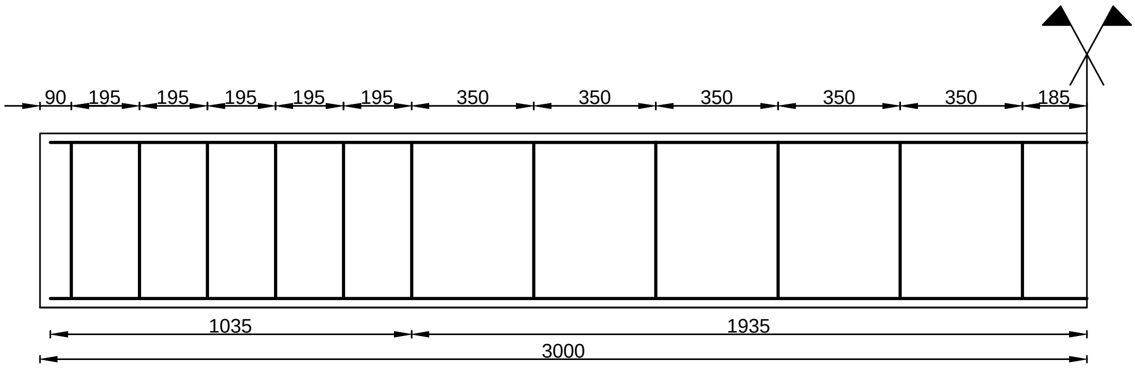

Figure 3.13. Transverse stirrups array along the beam.

3.4.2 Inclined rebars

This type of shear reinforcement is usually supplied because the principal tensile stresses act in an inclined direction with respect to the horizontal (see Figure 3.9 b)). Hence, their effectiveness increases by a certain amount. However, as specified earlier, in case of earthquakes they are more detrimental than vertical stirrups because in this case the load reversals are causing cracks parallel to the inclined reinforcement as the principal stresses change direction. This leads to zero reinforcement in beam that could be capable of handling these stresses. As a result cracks develop faster and the beam resistance decreases.

The involved relations for inclined reinforcement are derived in a similar way to those used for transverse shear reinforcement. Thus, the vertical tension carried by the stirrups is replaced by a uniform tension inclined at an angle to the horizontal, usually denoted by α. This angle is not necessarily equal to the one illustrated in Figure 3.9 b) as its value depends on the way the inclined stirrups are placed. Once more, the minimum value of shear resistance obtained from the two relations given by Equation (3.27) is taken into account [EN1992-1-1, 2014].

$$\begin{aligned} V_{Rd,s} &= \frac{A_{sw}}{s} z f_{ywk} \left(\cot\theta + \cot\alpha\right) \sin\alpha \\ V_{Rd,max} &= \alpha_{cw} b_w z \nu_1 f_{ck} \frac{\cot\theta + \cot\alpha}{1+\cot^2\theta} \end{aligned} \tag{3.27}$$

The same spacing between the shear reinforcement is kept as for the transverse case, while the angle α is chosen equal to 60° and the layout of the beam can be seen in Figure 3.14.

In Table 3.8 it is noticed that the shear resistance of the structural element increases even more than for the case of vertical stirrups and as a consequence the bearing capacity also increases. As expected, a beam reinforced with steel bars that account for shear force exhibits a better response to external loading than one without. Furthermore, this increase might seem rather large as opposite to the section presenting transverse reinforcement, but for further comparisons it is considered nevertheless.

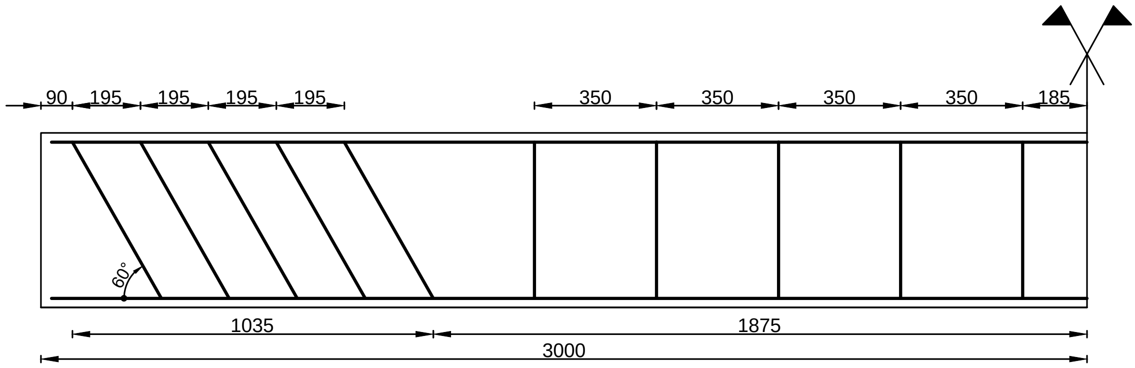

Figure 3.14. Inclined stirrups beam representation.

Table 3.8. Analytic results for inclined reinforcement.

V_{Rd} [KN]	$q_{cap}\left[\frac{\text{KN}}{\text{m}}\right]$
133.68	44.56

Numerical analysis 4

In this chapter a finite element analysis is implemented in order to represent as close as possible the plasticity behaviour of concrete. This is relevant for the design of reinforced concrete elements in today's modern era. Moreover, the effect of different reinforced cross-section are analysed. For calculations please refer to [Enclosures-CD, Chapter 4].

4.1 Constitutive models

The current analytic calculations of reinforced concrete elements are time consuming and present many assumptions that affect the real behaviour under external loadings. Hence, certain FE computational softwares, like ABAQUS, can solve problems with a high degree of difficulty.

In this project the effect of two models are analysed on a simply-supported reinforced concrete beam. Three different cross-sections are considered for which different results are obtained and compared between each other. This is done in order to verify which constitutive model fits best the non-linear behaviour of the proposed heterogeneous beams. Moreover, for the current project tension is considered positive while compression negative.

4.1.1 Mohr-Coulomb model

The Mohr-Coulomb (MC) yield surface is defined by the friction angle and cohesion as stated by Equation (4.1) while Figure 4.1 a) show the corresponding deviatoric plane. MC is the most common constitutive model in FE analyses due to the fact that it requires few input parameters and can provide a first guide estimate. However, the main reason is that materials such as sand or concrete are strongly dependent on pressure effects and MC is the simplest available model which is capable of handling this kind of situations. As a remark, in this project the MC material model is described in deviatoric plane by the major and minor principal stresses, σ_1 and σ_3.

$$f_{MC} = k\sigma_1 - \sigma_3 - \sigma_c = 0 \tag{4.1}$$

where

σ_1, σ_3	principal stresses
σ_c	uniaxial compressive strength, $\sigma_c = 2c\sqrt{k}$
$\sigma_{t,MC}$	uniaxial tensile strength, $\sigma_{t,MC} = \dfrac{\sigma_c}{k}$
c	cohesion
k	friction parameter, $k = \dfrac{1+\sin\varphi}{1-\sin\varphi}$
φ	friction angle [°]

MC returns a biaxial tensile strength known as the apex coordinate, σ_{apex}, which can not be measured with the current testing machines. Moreover, the MC uniaxial tensile strength, which is actually accounted as a material parameter, is larger than in reality and thus the resistance can be overestimated. In the present project this value is calculated as specified earlier and its representation can be seen in Figure 4.1 b). Thus, in order to avoid for such situations the original formulation of MC is modified by including the Rankine plasticity condition which allows for the reduction of the tensile strength of the material. This condition is termed "tension cut-off" and is given by Equation (4.2). Thus, it represents the highest possible tensile stress of the material.

$$f_{Rankine} = \sigma_1 - \sigma_t \tag{4.2}$$

where

σ_t	actual tensile strength of material

The tensile strength can be reduced by specifying the correct value of σ_t for the material to be analysed. The obtained result is highlighted in Figure 4.1 b). Thus, once $c\cot\varphi > \sigma_t$ the designated value is automatically set to σ_t.

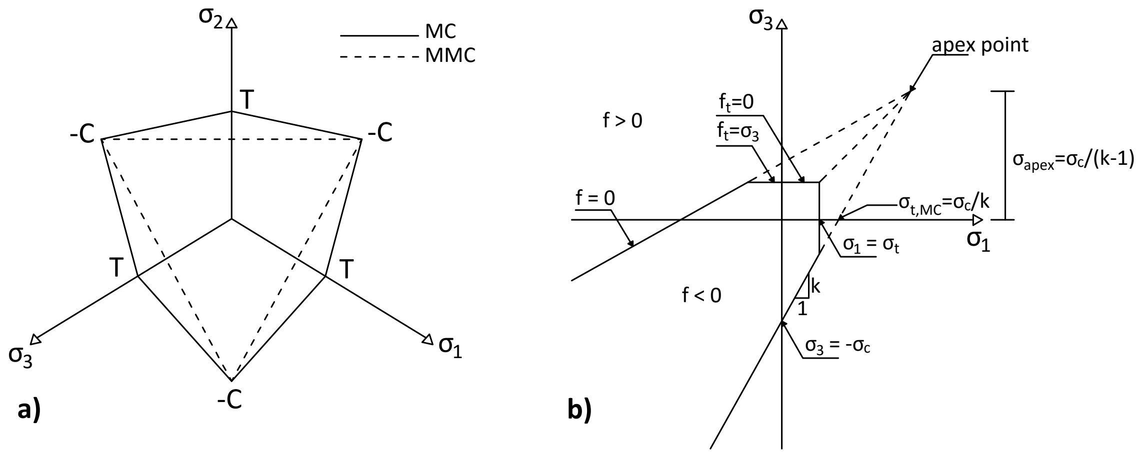

Figure 4.1. Projection of MC and MMC yield surfaces a) In deviatoric plane b) Into the $\sigma_1 - \sigma_3$ plane [Niels Saabye Ottosen, 2005].

When both Rankine and MC criteria are used together the resultant model is known as Modified Mohr-Coulomb (MMC). This is illustrated in Figure 4.1 a) in the deviatoric plane, where the Rankine part of the criterion, Equation (4.2), is taken to be associated while the Mohr-Coulomb part is non-associated.

Stress-strain relationship

MC model uses a linear elastic-perfectly plastic idealization of the real material behaviour. This can be seen in Figure 4.2, while concrete (see Figure 2.1 c)) presents high non-linearity during loading.

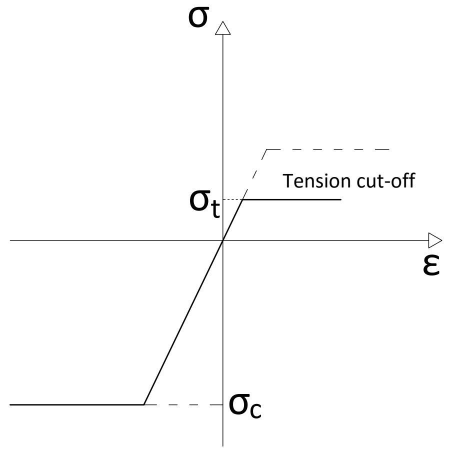

Figure 4.2. Idealized uniaxial stress-strain relationship of the MC model.

By the use of this model, concrete is represented with a linear-elastic behaviour in the elastic region, as defined by Hooke's Law, until it reaches plastic zone. MC model does not account for isotropic hardening as it is the case of real concrete behaviour which normally displays an increase in strength while plasticity takes place.

Material parameters for MC

The description of MC constitutive model is given by the parameters shown in Table 4.1. The cohesion is found as described earlier and is considered in the numerical analysis of the reinforced concrete beam. The friction angle is chosen as a recommended value for concrete [Y. Fujita, 1994]. However, the same paper proved that after some experimental measurements a major discrepancy has been observed and it is decided to test both values in a first simulation. Moreover, the dilation angle is given as default by Abaqus [2016], while the Poisson's ratio is recommended to be close to 0.20 [EN1992-1-1, 2014].

Table 4.1. Input parameters for the MC model.

Symbol	Description	Value	
σ_c	Uniaxial compressive strength	25 MPa	
φ	Friction angle	37 °	55 °
k	Friction parameter	4.02	10.06
ψ	Dilation angle	31 °	
E_{cm}	Secant Young's Modulus	0.315×10^5 MPa	
ν	Poisson's ratio	0.18	

Both, the standard MC and modified MC, models are investigated for the singly reinforced section and the one with the most satisfying results is treated for the other beam cross-sections as well.

4.1.2 Concrete Damage Plasticity model

ABAQUS introduced a new constitutive model under the name of Concrete Damage Plasticity (CDP). According to the provided documentation, CDP is capable of solving sophisticated problems that involve either plain and/or reinforced concrete structures. Hence, it can be used to model rebars as reinforcing material for concrete which makes it the first option when such situations are of concern [Abaqus, 2016]. Contrarily to MC, the deviatoric plane of the CDP model is chosen for this report to be described by the σ_1 and σ_2 principal stresses as this relates with the standard used notation in the analytic calculations of a concrete member.

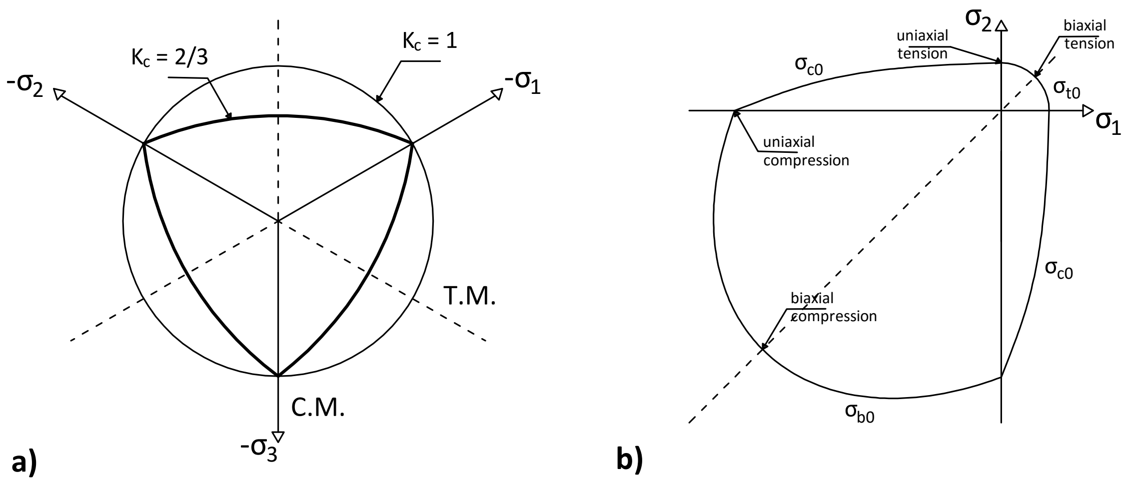

Figure 4.3. Projection of CDP yield surface a) In deviatoric plane b) Into the $\sigma_1 - \sigma_2$ plane [Abaqus, 2016].

The CDP model has a modified Drucker-Prager criterion and the yield surface in the deviatoric plane is visible in Figure 4.3 a) while the corresponding one for the plane stress can be seen in Figure 4.3 b).

CDP yield function is defined by Lublinier [1989] with corrections from Jeeho Lee [1998] to account for different effects in the evolution of strength under compression and tension. The yield criterion is given by Equation (4.3) and the corresponding yield surface evolution is controlled by the hardening variables $\dot{\varepsilon}_t^{pl}$ and $\dot{\varepsilon}_c^{pl}$.

$$
\begin{aligned}
f &= \frac{1}{1-\alpha}\left(q - 3\alpha p + \beta\left(\dot{\varepsilon}^{pl}\right)\sigma_{max} - \gamma(-\sigma_{max})\right) - \sigma_c\left(\dot{\varepsilon}_c^{pl}\right) = 0 \\
\alpha &= \frac{\left(\dfrac{\sigma_{b0}}{\sigma_{c0}}\right) - 1}{2\left(\dfrac{\sigma_{b0}}{\sigma_{c0}}\right) - 1} \quad , \quad 0 \leq \alpha \leq 0.5 \\
\beta &= \frac{\sigma_c\left(\dot{\varepsilon}_c^{pl}\right)}{\sigma_t\left(\dot{\varepsilon}_t^{pl}\right)}(1-\alpha) - (1+\alpha) \\
\gamma &= \frac{3(1-K_c)}{2K_c - 1}
\end{aligned}
\tag{4.3}
$$

where

σ_{max}	maximum principal effective stress
$\frac{\sigma_{b0}}{\sigma_{c0}}$	ratio of initial equibiaxial compressive yield stress to initial uniaxial compressive yield stress
K_c	ratio of the second stress invariant on the tensile meridian, $q_{(TM)}$, to that on the compressive meridian, $q_{(CM)}$, at initial yield for any pressure, p
$\sigma_t\left(\dot{\varepsilon}_t^{pl}\right)$	effective tensile cohesion stress
$\sigma_c\left(\dot{\varepsilon}_c^{pl}\right)$	effective compressive cohesion stress

Stress-strain relationship

As opposite to the MC model, CDP is designed to deal with applications in which the material is subjected to either monotonic, cyclic or dynamic loading. So, it allows for stiffness recovery during load reversals [Abaqus, 2016].

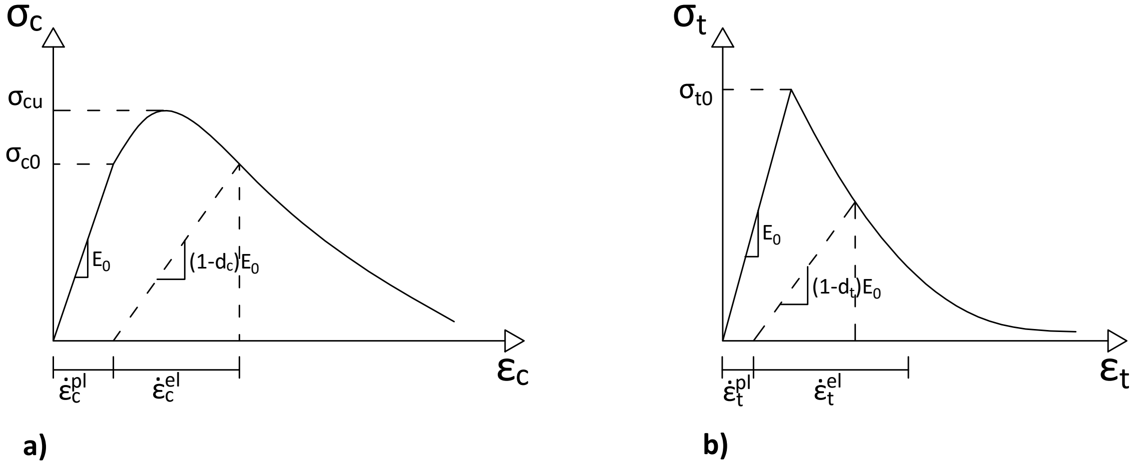

Figure 4.4. Concrete response to uniaxial loading in a) Compression and b) Tension.

During uniaxial compression the stress-strain response is linear up to the initial yield point, σ_{c0}. Afterwards, when entering the plastic region the response is represented by stress hardening which is later followed by strain softening beyond the ultimate stress, σ_{cu}.

Under uniaxial tension the response is linear-elastic up to the value of the failure stress,σ_{t0} which corresponds to the onset of micro-cracking in the concrete material. Beyond the failure stress the formation of cracks in the tensioned zone is represented with a softening stress-strain response, which induces strain localization (jumps) in the concrete structure.

Material parameters for CDP

CDP is an advanced constitutive model and as a result requires more parameters than MC. In order to obtain realistic values for some parameters experiments must be performed beforehand. Thus, due to lack of measurements, default values, as indicated in [Abaqus, 2016] documentation manual, are considered for these specific ones.

Table 4.2. Input parameters for the CDP model.

Compression Hardening Law		Symbol	Description	Value
σ_c [MPa]	ε_c^{pl}			
12	0.00018	σ_{t0}	Yield stress in tension	2.16 MPa
13	0.00020	ε_t^{pl}	Tensile plastic strain	0
14	0.00023	ψ	Dilation angle	31 °
15	0.00026	e	Eccentricity	0.1
16	0.00029	$\frac{\sigma_{b0}}{\sigma_{c0}}$	Tatio of stresses	1.16
17	0.00033	K_c	Tatio of the stress invariants	0.667
18	0.00037	μ	Viscosity Parameter	0
19	0.00042	E_0	Young's Modulus	3.15×10^4 MPa
20	0.00047	ν	Poisson's ratio	0.18
21	0.00053	d_c	Compressive damage variable	[-]
22	0.00061	d_t	Tensile damage variable	[-]
23	0.00070		**Proposed tension softening law**	
24	0.00084	σ_t [MPa]	ε_t^{pl}	
25	0.00121	2.16	0	
24	0.00164	1.44	0.00025	
23	0.00206	0.81	0.00056	
22	0.00250	0.36	0.00104	
21.25	0.00283	0	0.0016	

The hardening and softening laws for the concrete response in compression and tension respectively are obtained as specified in Section 2.1.1. Moreover, the hardening law shown in Table 4.2 contains only the values from stresses equal to 12 MPa, but in the numerical simulations this law starts from a value of the stress equal to zero. However, as CDP model shows in Figure 4.4 a) a linear variation of the response up to σ_{c0}, the range indicated in Table 4.2 can as well be considered a good approximation.

4.2 Singly reinforced beam

Having already established with the aid of ACI318M [1995] and EN1992-1-1 [2014] the moment capacity, bearing capacity and displacement at the mid-point of a concrete beam with steel reinforcement placed in the tensile zone, as well as other output parameters, next a more thoroughly investigation is wanted. So, in order to perform a comparison between the available code procedures and the FE powered computer softwares like ABAQUS the reinforced concrete beam is modelled and afterwards simulations are carried out in order to obtain the necessary output data.

4.2.1 Geometry

The rectangular concrete beam is modelled as a 3D deformable solid body as seen in Figure 4.5. First, the associated material type is that of homogeneous plain concrete for which the material parameters stated in Table 4.1 and Table 4.2 are considered for the MC and CDP model respectively.

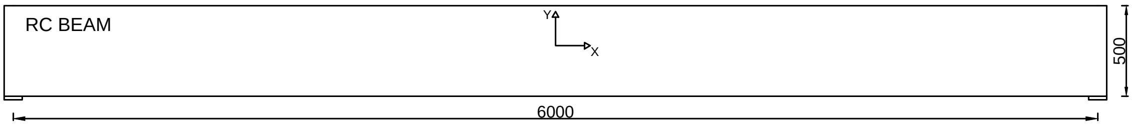

Figure 4.5. Illustration of the considered beam.

The steel reinforcement is modelled in two different ways, mainly a first technique is the same as the one used for the concrete cross-section and is visible in Figure 4.6 a). Hence, the steel bars can be merged directly with the concrete without requiring any contact constraints. The second applied method is with the use of a 3D deformable wire element which can be seen in Figure 4.6 b). For this reason the rebars are now embedded inside of the concrete material which is the host body. Moreover, for the wire type, a cross-section equal to the diameter of the considered longitudinal bars is implemented in ABAQUS.

An idealised behaviour, as depicted by Figure 2.5 c), is considered for steel and the considered material parameters can be found in Table 4.3. Thus, the plasticity associated with it is that of a ductile material assumed by Von Mises yield criterion.

Table 4.3. Steel input parameters.

Symbol	Description	Value
f_{yk}	Yield strength of steel	345 MPa
ε_{pl}	Plastic strain	0
E_s	Young's Modulus	2.1×10^5 MPa
ν	Poisson's ratio	0.3

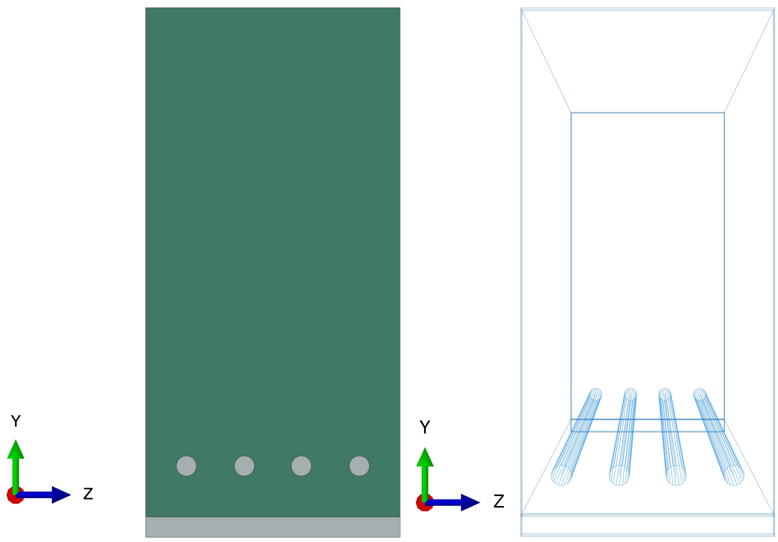

Figure 4.6. a) Solid steel bars and b) Wire steel bars.

4.2.2 Boundary conditions and symmetry

As stated in Chapter 3 the beam is simply-supported. Thus, in one of the ends the beam has a hinge which constraints translations on x- and y-directions. Moreover, in the other end a simple support restraining translations in the y-directions is imposed.

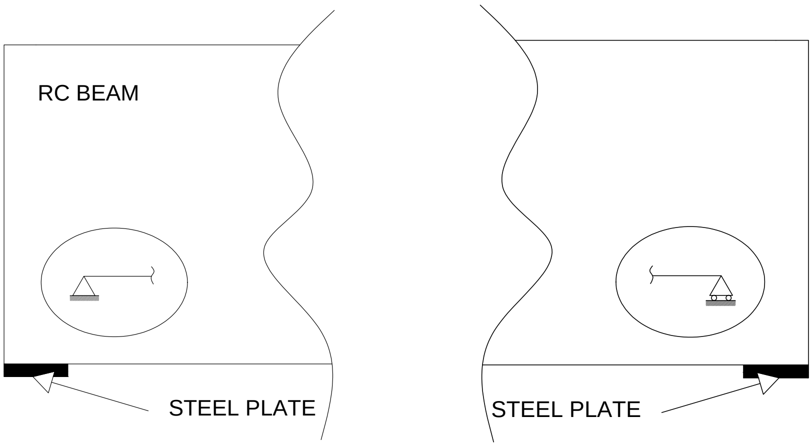

Figure 4.7. a) Hinge support b) Simple support.

In ABAQUS these support conditions are modelled as steel plates for which the same material as for the reinforcement is considered. The actual constraints are inserted along the width of the beam on a line placed on the middle of the steel plates. This representation is visible in Figure 4.7 a) and 4.7 b).

The applied loads visible in Figure 4.8 are modelled as surface pressure load with a uniform distribution. Thus, the actual loads obtained in the analytic calculations, for both SLS and ULS cases, are divided by the actual width of the beam.

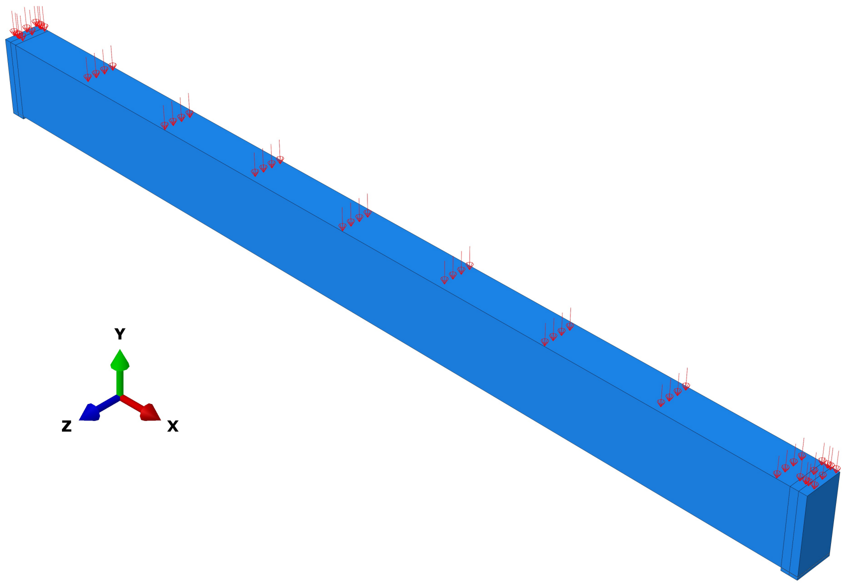

Figure 4.8. Uniform loads acting on the beam.

Since FE commercial softwares can be high demanding in computational time two symmetry planes are taken into consideration. The first one is placed in the center of the beam along its width. For this symmetry plane a constraint along the x-axis is consider in order to obey same principles as the actual beam. Moreover, a second plane is considered along the length and here the translation along the z-axis is contrained. The result together with its considered constrains is visible in Figure 4.9.

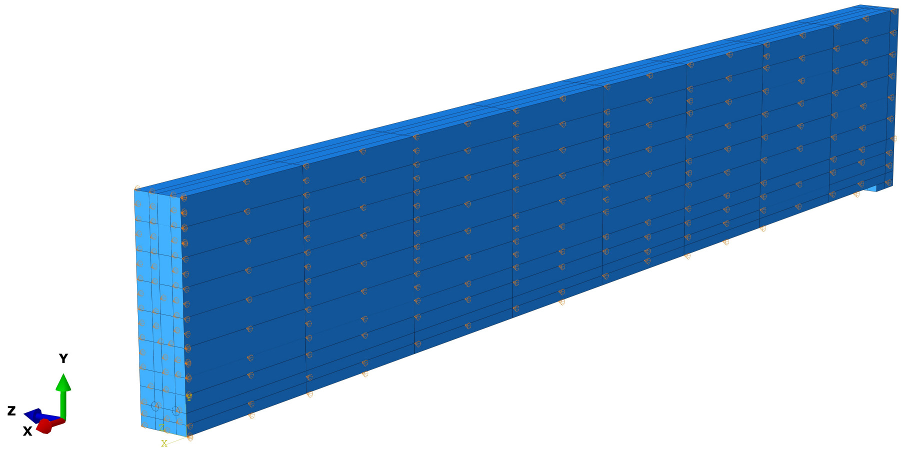

Figure 4.9. Beam after application of symmetry planes.

4.2.3 Meshing and convergence analysis

The basis of every FE numerical products is the discretization of the considered model in a number of elements. A mesh (see Figure 4.10) is typically a network of lines that connect between each other with a certain amount of nodes used to numerically solve the problem at stake under external loadings. Thus any internal efforts like, axial force, shear force or bending moment can be calculated accurately. This is however strongly connected to the number of nodes involved and furthermore with the number of degrees of freedom of each node.

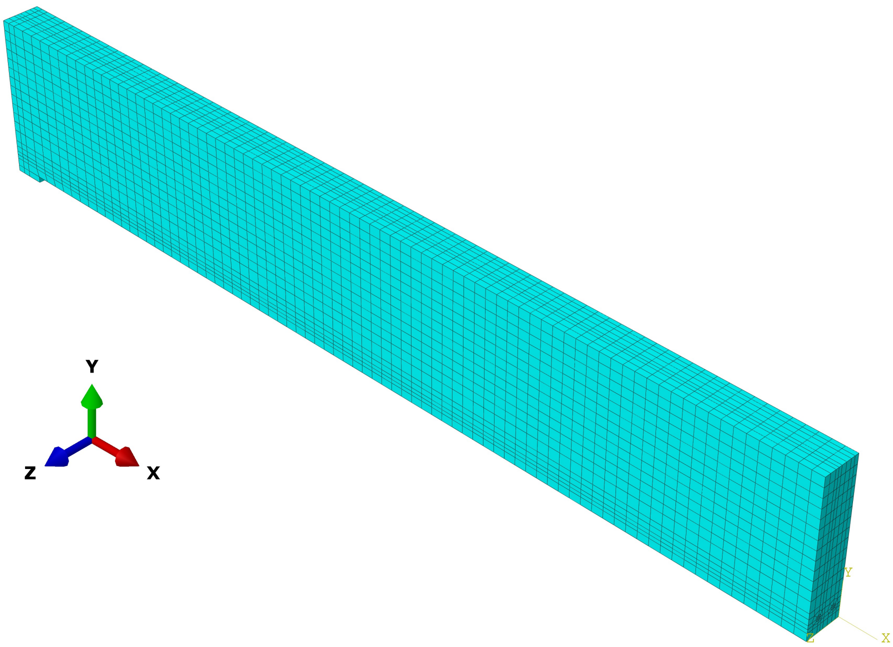

Figure 4.10. Applied mesh for the RC beam.

In the present project, as it is visible in Figure 4.11, the concrete beam is meshed using Hex elements, namely C3D8R, which is a 8-node linear brick having only one integration point. This can be both an advantage and a disadvantage in the same time, as it decreases CPU power and duration of the analysis, but for a proper result in terms of stresses and strains more integration points are better. Thus, in order to check the accuracy of the results a sensitivity analysis is performed using an element type C3D8 which has four integration points and the results can be seen in Figure B.4. The steel reinforcement is meshed in two different ways, either by C3D8R as for the concrete, or with T3D2 elements in case of wires. The later is known as a 2-node linear 3D truss.

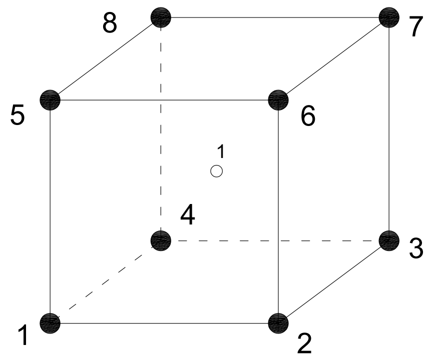

Figure 4.11. C3D8R hexahedral element.

So, a higher discretization can lead to better results while a weaker one can save computational time which lead to the fact that a compromise must be made between the two. For these reasons, a convergence analysis is performed on the bottom fibre of the beam at mid-span. The point is chosen at this location due to the fact that in the analytic calculation the same point was chosen. Different element sizes are chosen and the corresponding displacement is afterwards simulated.

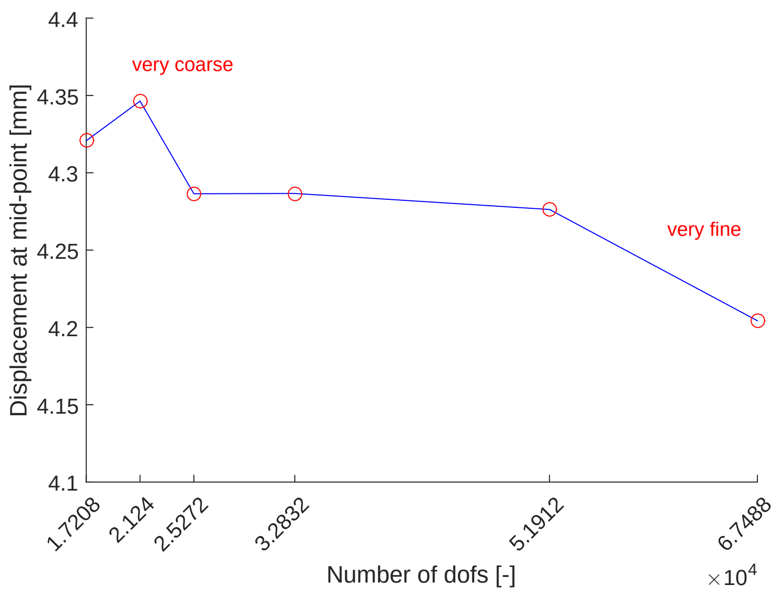

Figure 4.12. Convergence analysis. Imposed load equal to 15 KN. Reinforcement modelled as solid elements.

Thus, a convergence analysis is shown in Figure 4.12. Due to a rough amount of partitions imposed, the element sizes might actually differ from place to place and for a proper convergence the sizes should be constant along the entire model. However, it is distinguished that the difference in the results is very small, and so it is concluded that an element of medium size can be chosen without any major discrepancies in the results.

4.2.4 MC analysis

Since MC is a relatively simple model and requires few input parameters the actual behaviour of the material under loading might not be accurately captured. When analysing a reinforced concrete structural element it is necessary to ensure that reliable concrete parameters are taken into account and that the obtained data is authentic.

Friction angle influence on concrete behaviour

Present papers indicate different values for the actual friction angle of concrete. In general it is recommended to use a value of 37 °, but current experiments indicated a much higher internal angle of friction, mainly 55 ° [Y. Fujita, 1994]. Thus, the input parameters suggested in Table 4.1 are used and the results are investigated for the actual response of concrete when subjected to external loads.

A first analysis is carried for the SLS case where the displacements against a load of 15 KN are calculated and checked. From Figures 4.13 is visible that a friction angle with a value of 37 ° gives a smaller displacement when comparing to larger angles. Concrete material is defined by both compressive and tensile strengths. Hence, according to Equation (4.1), for a lower angle of internal friction MC returns a higher tensile strength. This means that the actual resistance is overestimated and one could argue that stiffness is also increasing, resulting in lower deformations. [Det Norske Veritas, 1992] states that a relationship exists between the Poisson's ratio and friction angle of the material and this is represented by Equation (B.1). However, the empirical relationship was developed for soils and is used only as a guideline.

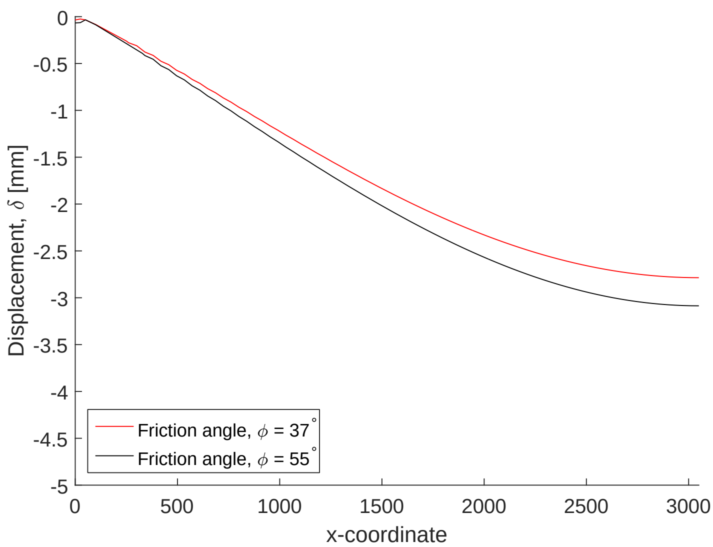

Figure 4.13. Displacement comparison between different friction angles. Reinforcement modelled as wire elements.

Due to the small difference in displacement between the two models further analyses are required in order to see which of them represent concrete behaviour best, and these are presented next.

For a comparison in terms of ULS certain analyses are conducted in order to ensure that beam reaches failure when using either of the two friction angle values. Firstly, the plastic strains are pictured in Figure 4.14 as contour plots. As expected, these are localised on both compressive and tensile fibres where failure in concrete occurs due to crushing and cracking respectively. Figure 4.14 b) again return higher values, but the strains spread in the same manner for both cases which emphasise an approximate behaviour.

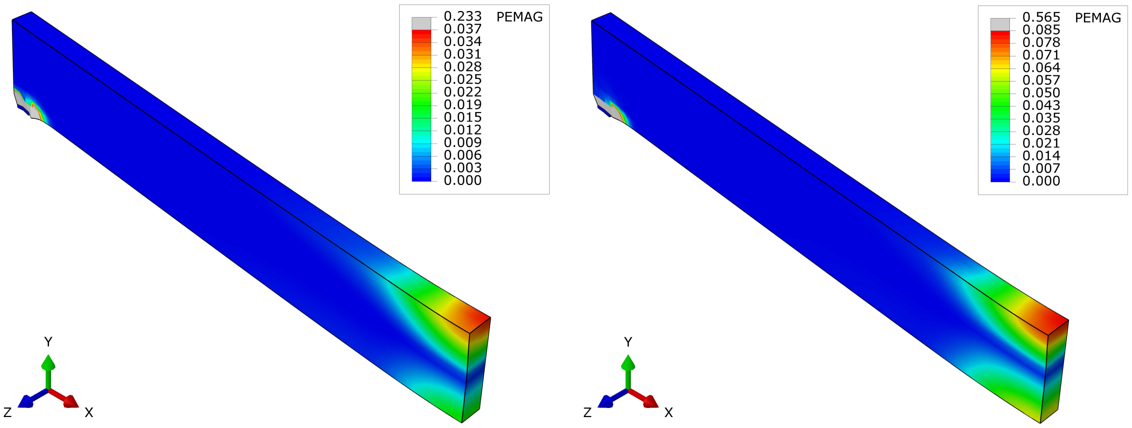

Figure 4.14. Plastic strains regions in a beam with a) friction angle of 37 ° and b) friction angle of 55 °. Reinforcement modelled as wire elements.

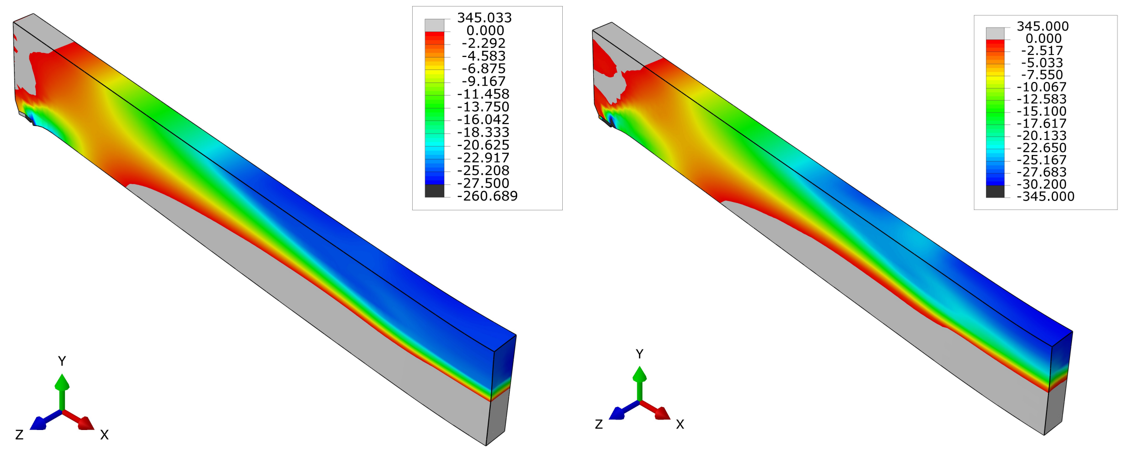

Figure 4.15. Compressive stress of concrete with a) friction angle of 37 ° and b) friction angle of 55 °. Reinforcement modelled as wire elements.

Secondly, when investigating the compressive and tensile stresses in the concrete at failure (see Figures 4.15 and 4.16), different friction angles can give both good and bad estimates. Once more, a higher friction angle overestimates the actual compressive strength of concrete returning a value by 17% higher than the actual one of 25 MPa, while when considering a friction angle of 37 ° it is overestimated by only 9%, which anyway can still be dangerous if design of concrete structures by the use of MC model is performed. When evaluating only the tensile strength of concrete it is visible in Figure 4.16 b) that the stress in the beam is very close to the real one of 2.16 MPa, as opposite to the model which uses a friction angle of 37 °. The latter overestimates the actual strength by quite a margin having a value almost three times the real one. Moreover, Figure 4.16 a) show a tensile stress spreading over a larger portion which in reality usually does not occur.

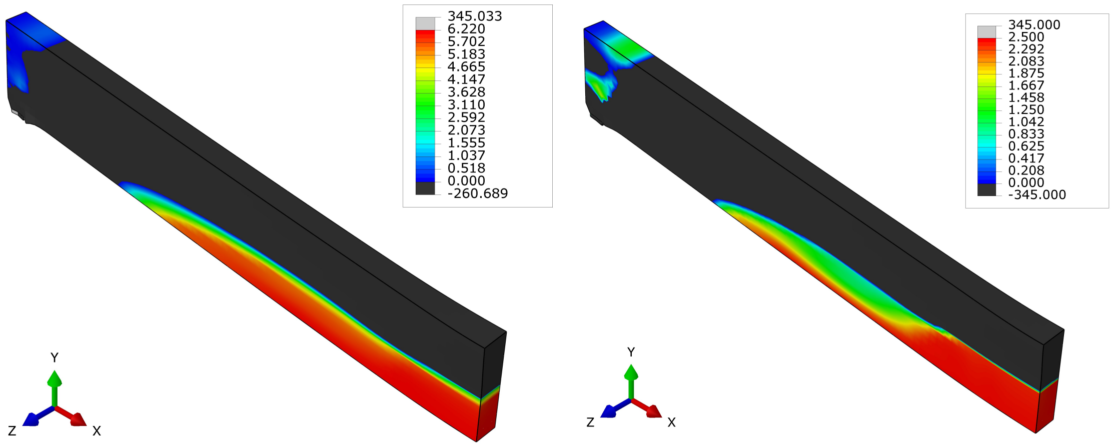

Figure 4.16. Tensile stress of concrete with a) friction angle of 37° and b) friction angle of 55°. Reinforcement modelled as wire elements.

Tensile strength effects on concrete response

As specified earlier in Section 4.1.1, the modified MC constitutive model takes into account tension cut-off which can reduce in the end the tensile strength of concrete to its proper value. Thus, a model with a friction angle of 37° together with a correct input for tension cut-off stress should return a stress-strain relationship close to the one shown in Figure 4.2. However the model crashed when simulations were performed in order to obtain a sensitivity analysis of concrete under different tensile stresses. This can be attributed to an error in the ABAQUS programming code of the MC model when the tension cut-off option is turned on.

The load-displacement curve is constructed for both values of friction angle and can be seen in Figure 4.17. The ultimate load at failure differs by a margin, with higher values for the case which considers a lower angle of internal friction. Moreover as specified earlier, it can be seen that the slope of the curve increases by a small amount which leads to the fact that up to a certain degree a correlation must exist between the angle of internal friction and stiffness of the material.

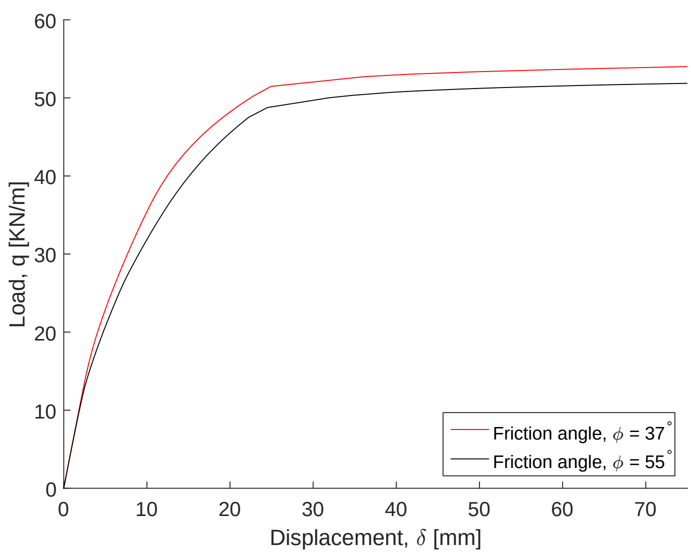

Figure 4.17. Displacement-load graph for MC model with different friction angles. Reinforcement modelled as wire elements.

Further considerations

Since available theoretical studies together with experimental measurements show uncertainties on the actual friction angle of concrete more research has to be performed if the actual FE modelling of concrete structures by the use of MC is desired. As mentioned earlier it is implied that concrete exhibits a response under an angle of internal friction of 37 °, but as demonstrated the bearing capacity can actually be overestimated if the use of MC model without tension cut-off is considered. Hence, due to the fact that in the current case this option is unapproachable, alternative ways of accurately defining concrete are investigated and these can be seen in Figure 4.18.

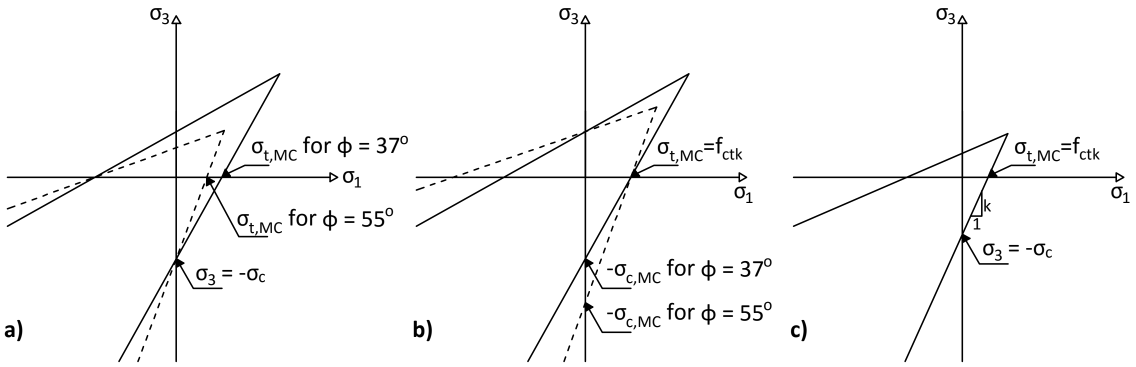

Figure 4.18. Alternative methods of describing concrete behaviour by use of MC model.

While Figure 4.18 a) is the one which was accounted for earlier, two other different approaches are analysed. Firstly, as illustrated by Figure 4.18 b), one possibility is to limit the MC uniaxial tensile strength to the actual tensile strength of concrete and with respect to different friction angles to model the structural element. However, if the chosen concrete class has a higher compressive strength of concrete and the use of $\varphi = 37°$ is to be used the bearing capacity could be underestimated, and viceversa for a lower compressive strength together with a higher friction angle. Since both f_{ck} and f_{ctk} are given while φ is assumed, a third option as shown in Figure 4.18 c) can be implied. Thus, limiting both σ_1 and σ_3 stresses to the compressive strength of concrete and its tensile strength respectively, the friction parameter can be calculated and afterwards the angle of internal friction for the corresponding concrete class based on MC criterion is found. The analysis is performed for cases b) and c) since they are considered to be the most appropriate ones and the bearing capacity of each is shown in Figure 4.19.

As expected, a combination of smaller friction angles with an imposed MC uniaxial tensile strength equal to the one of concrete estimates a bearing capacity almost half of the real one. At the same time using the approach illustrated in Figure 4.18 b), but for the largest friction angle, it is observed that the bearing capacity is actually much closer to the analytical calculated one. When fixing both the compressive and tensile strength of concrete on the MC envelope (see Figure 4.18 c)) it seems that the in-built ABAQUS MC material model is not capable of handling friction angles of greater magnitudes, as the one which is calculated and used as input parameter equals 57.3°. A very small increment size might solve this issue, but as shown the bearing capacity would be overestimated anyway when comparing to "case b) $\varphi = 55°$".

For the simple purpose of further investigations and comparisons, the MC model with a friction angle equal to 55 ° is used in all of the proposed reinforced concrete beam sections.

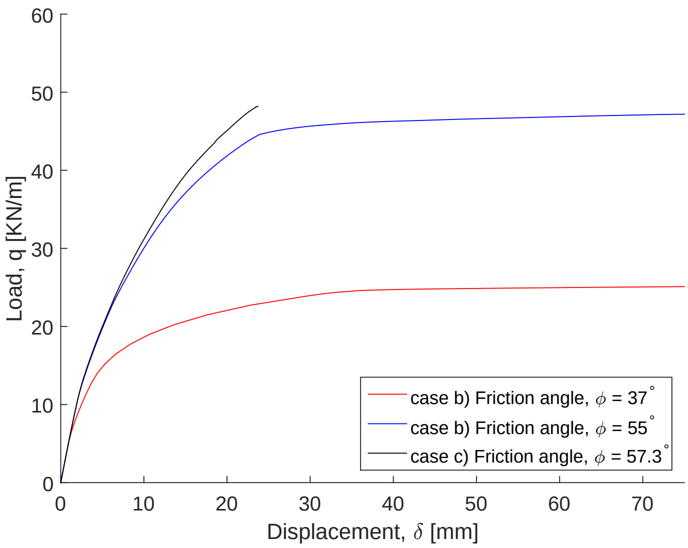

Figure 4.19. Displacement-load graph for MC model by using different approaches. Reinforcement modelled as wire elements.

Results

In order to validate the results for the SLS, when using a load of 15 KN, the same plot as depicted by Figure 4.14 is constructed again. By looking at Figure B.5 it is clearly visible that no plastic strains can be found in the beam which proves that the chosen load for SLS analysis is a good assumption and the material might behave in a linear-elastic manner.

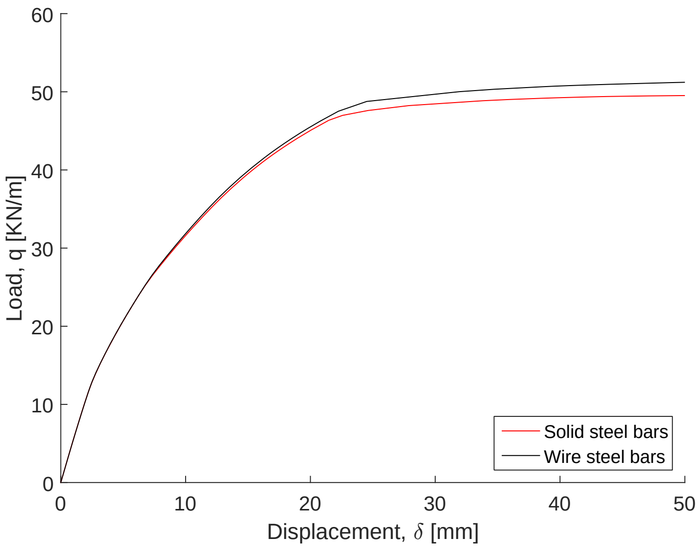

Figure 4.20. Load-displacement of a beam modelled with solid and wire rebars.

The load-displacement curve for the two cases with reinforcement modelled as either solid or wire elements is visible in Figure 4.20. The bearing capacity of the beam is overestimated by the use of wire elements, while the displacement is by a small margin lower than for the case of solid rebars. The output results are given in Table 4.6.

Table 4.4. FE analysis results.

Type of bars	δ [mm]	M_{cap} [KNm]	q_{cap} $\left[\frac{\text{KN}}{\text{m}}\right]$
	SLS	ULS	
Solid	3.09	224.41	49.87
Wire	3.08	233.41	51.87

4.2.5 CDP analysis

In ABAQUS a rough simulation of the CDP model can be performed, meaning that only the strength input parameters at failure are specified, f_{ck} and f_{ctk}, for which their corresponding plastic strain value is zero. No hardening nor softening takes place and as such, the laws given in Table 4.2 are not specified. By doing so, an idealised concrete behaviour close to that of the MMC constitutive model, and visible in Figure 4.2, results. Hence, a separate analysis is performed in order to investigate the differences between an idealised behaviour of concrete and the two proposed in Figure 2.4 a) and b).

Effects of hardening and softening laws on the response

The stress-strain curve involved for the hardening behaviour is the one represented by Figure 2.4 a). A first investigation in terms of displacements is performed for the SLS case. Figure 4.21 show the different results obtained for the two different adopted methods. It is clearly visible that for the model which takes into account the hardening law an increased displacement compared to the idealised case is achieved. This means that in reality, under same load magnitudes, concrete deforms more. Thus, too many assumptions made on the actual stress-strain relationship will lead to a bad design in the end as the displacement is going to be underestimated. Contour plots of the displacement are shown in Figures B.2.

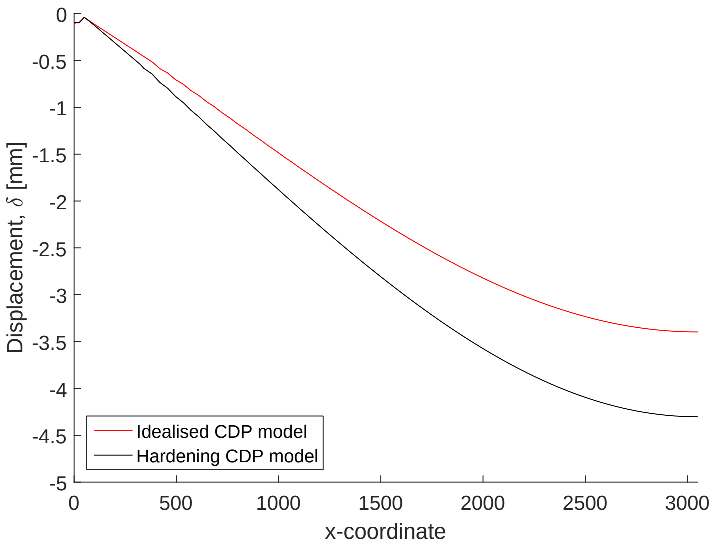

Figure 4.21. Displacement comparison between idealised and hardening behaviour models. Reinforcement modelled as solid elements.

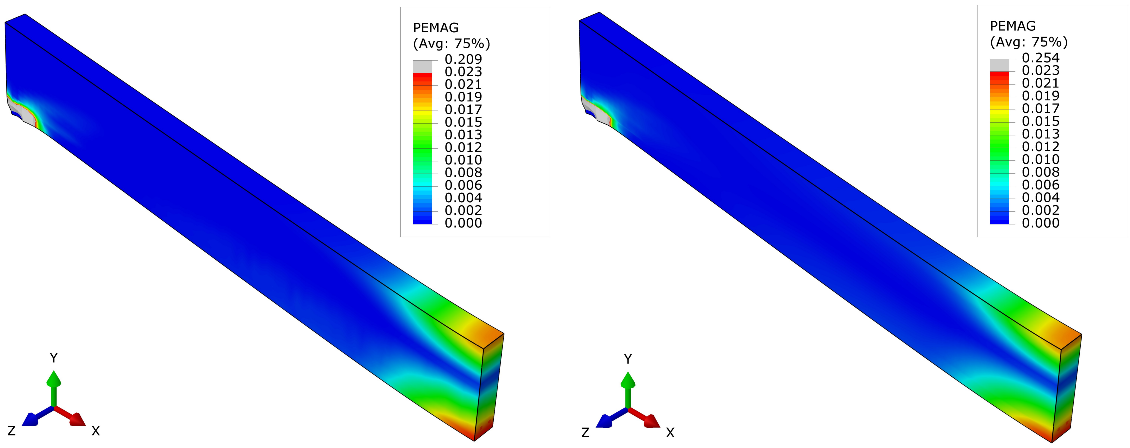

Figure 4.22. Plastic strains regions in a) idealised behaviour model and b) in hardening behaviour model. Reinforcement modelled as solid elements.

When looking at ULS, an investigation is carried out in terms of plastic strains and principal stresses for concrete. For the CDP model, the compressive crushing and tensile cracking of concrete are the fundamental failure mechanisms [Abaqus, 2016]. These two can be illustrated by Figures 4.22 a) and b), where the plastic strains are restricted to regions in the beam corresponding to the fibres under compression and tension effects. No significant difference is visible between the involved models and this can once again support the idea that hardening affects only the SLS scenario.

It is known from the chosen concrete strength class that the involved material can resist in compression until 25 MPa and in tension up to 2.16 MPa. So, in order to check only for stresses in concrete the scaling is modified accordingly. Both models seen in Figures 4.23 a) and b) correspond well at their ultimate state reaching a value of 27.5 MPa in the compressed zone. However, due to the imposed hardening law the stresses are distributed much more uniformly in the beam.

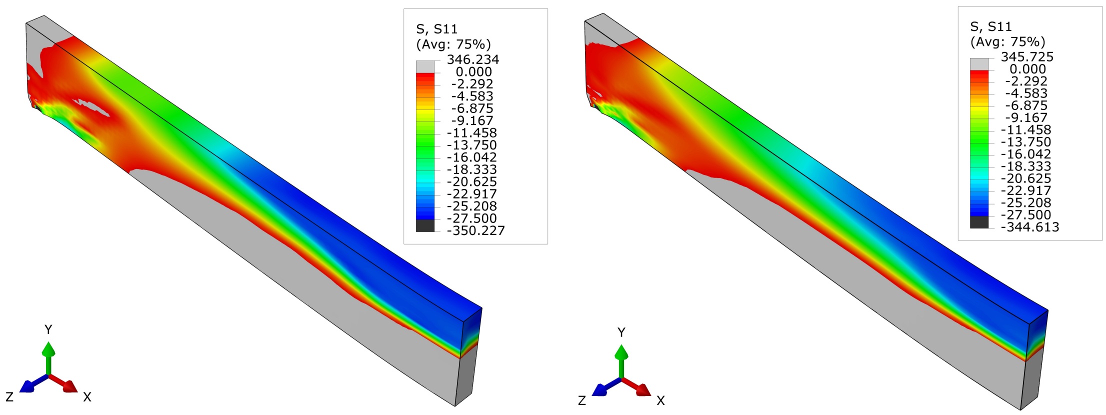

Figure 4.23. Compressive stress of concrete in a) the idealised model and b) in hardening model. Reinforcement modelled as solid elements.

The implementation of compression softening law recommended by Hognestad [1951] and tension softening stated by Bruno Massicotte and MacGregor [1990] respectively (see Figures 2.2 b) and 2.3) in ABAQUS gives a crash immediately after the start-up of the simulation. The main issue stands in the input parameters required for the CDP constituve model. Hence, it is due to the damage parameters, d_c and d_t, for the crushing and cracking zones of concrete which control the slope of the curve after reaching the peak value and are not included (see Figure 4.4). These parameters are very hard to obtain analytically and experimental measurements are required in advance.

However, by using this stress-strain curve which does not account for softening laws, Figures 4.24 a) and b) indicate a small difference in the way tensile stresses are located in the beam. In Figure 4.24 a) is seen a more localised spreading in the middle of the beam while the stresses in Figure 4.24 b) spread out more evenly.

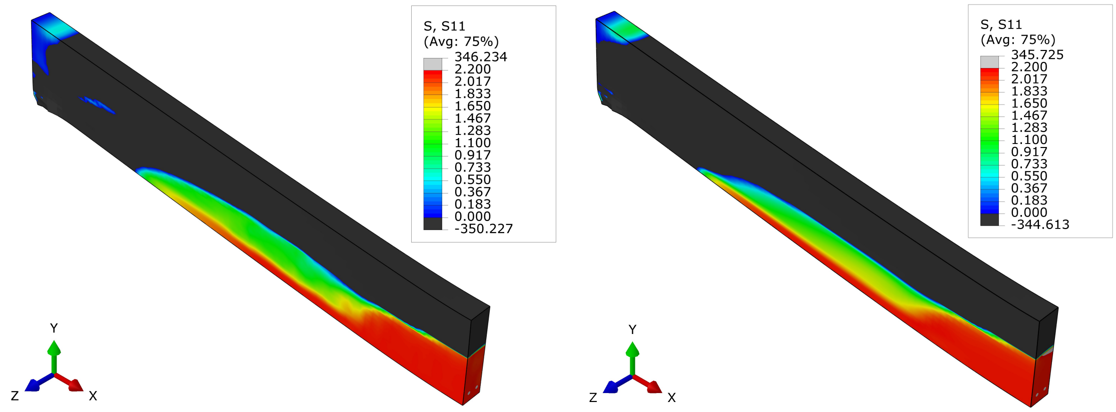

Figure 4.24. Tensile stress of concrete in a) the idealised model and b) in hardening model. Reinforcement modelled as solid elements.

To understand this behaviour in-depth, the load displacement curve is constructed for both approaches. Moreover, it must be mentioned that the presented trends are for a beam modelled with solid elements for the reinforcement. In Figure 4.25 it is seen that failure is reached in both cases and for the same value of ultimate load.

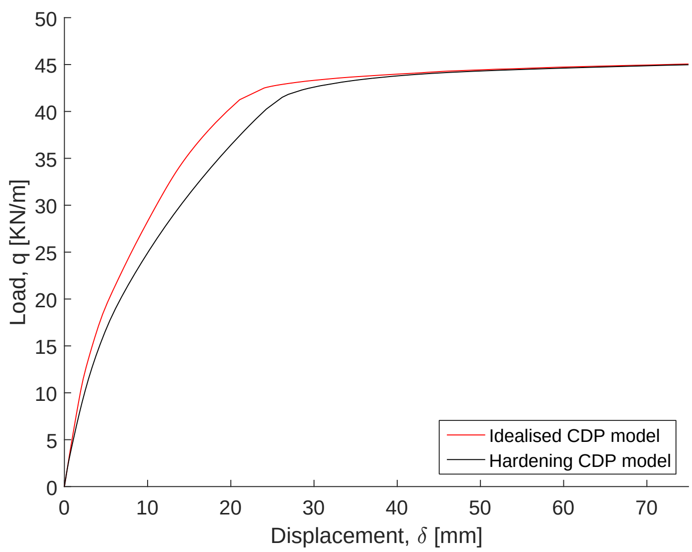

Figure 4.25. Displacement-load graph for idealised and non-linear stress-strain curves. Reinforcement modelled as solid elements.

The stress-strain curve is constructing based on the data obtained from the simulation results and can be seen in Figure 4.26. Stresses and strains have been chosen in the mid point of the beam, both on the upper and bottom fibres, in order to achieve an accurate representation of concrete behaviour by the two different analysed constitutive models. In ABAQUS, stresses and strains are given with respect to the axes of the beam, thus the plot is a σ_x - ε_x relationship. As expected, this concrete response resembles to the one given by EN1992-1-1 [2014] and shown in Figure 2.4 a).

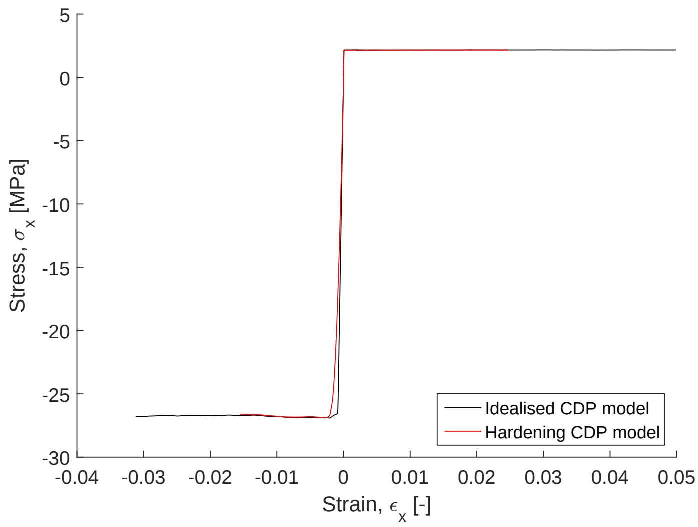

Figure 4.26. Stress-strain relationship of concrete, at mid-point, obtained from ABAQUS. Reinforcement modelled as solid elements.

It is noticeable that the last recorded point is at a higher strain value and as such the simulation process lasts longer for the idealised model than for the one which takes into account a non-linear variation of the stress-strain curve of concrete in compression.

Due to all of the observed phenomena, the calculations for all of the reinforced concrete cross-sections are performed using the CDP model which has the input parameters in terms of hardening. Moreover, it is noticed that the stresses in the steel reinforcement reach the imposed yielding limit for the ULS which agrees well with the conditions applied in the analytic calculations.

Results

The output results when using the hardening CDP constitutive model are visible in Table 4.5. They are different for the different ways used in the modelling process of reinforcement and Figure 4.27 show the bearing capacity of both.

It is clearly visible that when using wire rebars the beam has a higher resistance until failure, but the allowable displacement for the SLS case is smaller. Moreover, when looking at the model with solid rebars the reached value of bearing capacity agrees more with the one calculated analytically, while the achieved displacement is slightly higher.

Table 4.5. FE analysis results.

Type of bars	δ [mm]	M_{cap} [KNm]	q_{cap} $\left[\frac{\text{KN}}{\text{m}}\right]$
	SLS	ULS	
Solid	4.30	199.54	44.34
Wire	4.27	212.77	47.28

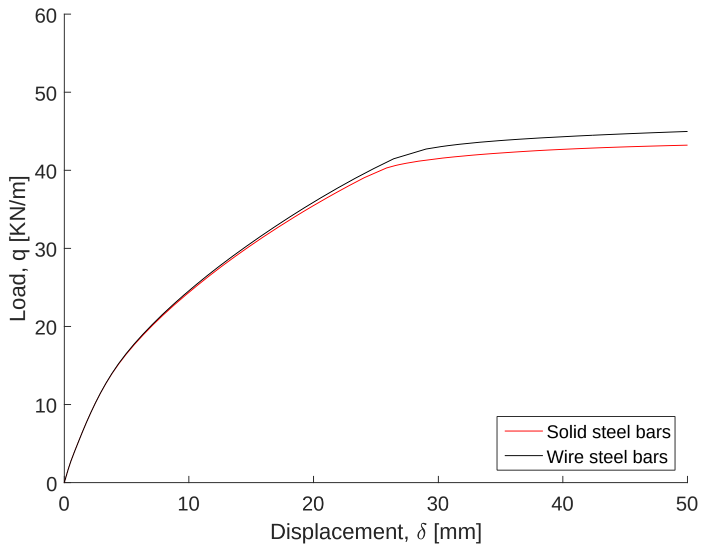

Figure 4.27. Load-displacement of a beam modelled with solid and wire rebars.

As a side note, during the calculations (ULS especially) it was observed that a high amount of straining occurred after reaching the yielding zone and as such the computational time was increased also. Thus, the option **nlgeom** which accounts for geometric non-linearity is switched on for the simulation process. Abaqus [2016] manual states that *"If the displacements in a model due to loading are relatively small during a step, the effects may be small enough to be ignored. However, in cases where the loads on a model result in large displacements, nonlinear geometric effects can become important."*

When the option is switched off, ABAQUS accounts that all calculations take place in the original reference model. Thus, when plasticity calculations are carried on and large deformations are expected, in order to distinguish between the reference undeformed model and the current deformed one it is best to consider **nlgeom**. An analysis in terms of bearing capacity is performed to see if this option affects the results and by how much and as seen in Figure B.3 the difference is slightly bellow 5%, but is important to point out that the simulation stops and no continuous deformation take place after reaching failure. However, since the analytic calculations are carried out in the original reference system and a comparison is desired, the nlgeom option is kept off.

4.3 Doubly reinforced beam

The effect steel bars placed in the compressed zone of the beam have on its behaviour is also analysed by means of the FE computational software ABAQUS.

4.3.1 Geometry

The same geometry as the one used in Section 4.2 for the singly-reinforced concrete beam is kept. Moreover, rebars are placed on the top part and again they are modelled as both solid and wire elements. A cross-section through the newly considered beam is shown in Figures 4.28 a) and b).

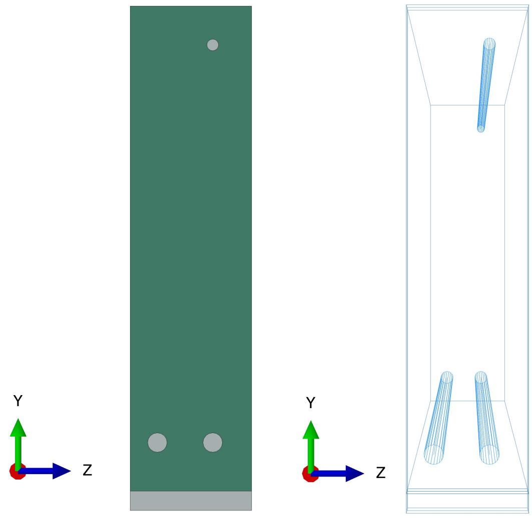

Figure 4.28. a) Solid steel bars and b) Wire steel bars.

The imposed diameter for the new rebars is of 12 mm and is chosen as such in order to comply with the yielding condition specified during the analytic calculations and in return to obtain an under-reinforced beam. Moreover, the same material properties given in Table 4.3 for the rebars placed in the bottom part are treated, with the only mention that the yield class of the compressed bars is S235 for the same reason as mentioned above.

4.3.2 Results

At first the SLS is checked in terms of displacements. As illustrated in Figure B.9 and B.10 the difference is insignificant with respect to the type of element used in modelling the reinforcement, while the difference becomes considerable between MC and CDP model.

With respect to the bearing capacity of beam, the same aspect as previously enunciated for the singly-reinforced beam is also observed in this case by Figure 4.29. It is noticeably that the value at which the beam fails is closer to the analytic calculations if bars are incorporated directly and if the same element type is used for both materials, steel and concrete. Otherwise, an increase by almost 4% is obtained which lead to bad designing. The results for the doubly reinforced beam are given in Table 4.6.

Table 4.6. FE analysis results.

Type of bars	δ [mm]	M_{cap} [KNm]	q_{cap} $\left[\frac{\text{KN}}{\text{m}}\right]$
MC model	SLS	ULS	
Solid	3.03	229.59	51.02
Wire	3.00	238.06	53.08
CDP model	SLS	ULS	
Solid	4.16	201.96	44.88
Wire	4.11	217.57	48.35

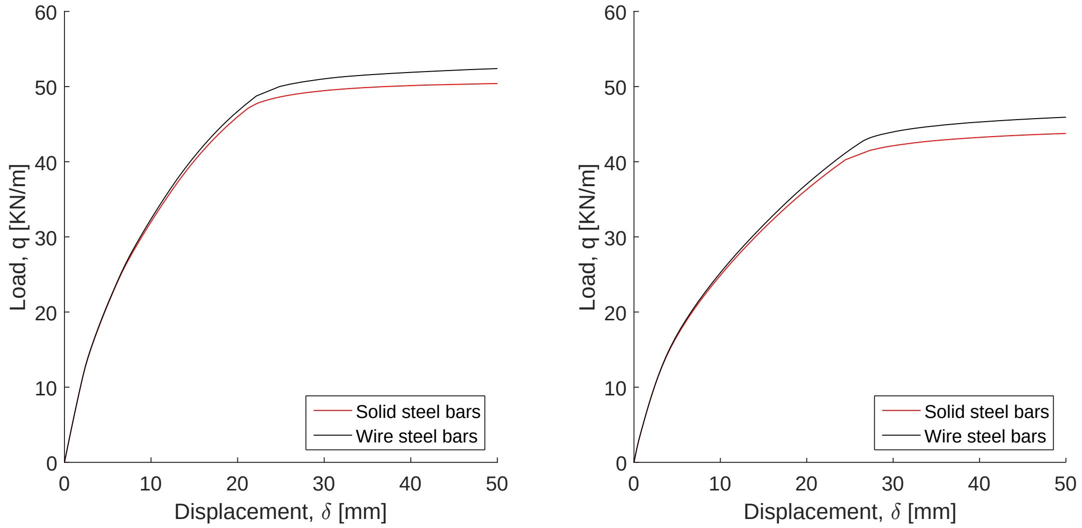

Figure 4.29. Load-displacement of a beam modelled with either a) MC model or b) CDP model.

4.4 Effect of shear reinforcement

In ABAQUS the only possible way of modelling this type of reinforcement is by using wire elements, as imposing both the diameter and the shape of the stirrup at the same time is not achievable for a solid body element. Hence, according to the analyses performed for wire rebars in Sections 4.2 and 4.3 a less conservative case is going to be obtained. The imposed bar geometry and material properties for shear reinforcement, in the FE analyses, are those prescribed in Section 3.4. Thus, based on the analytic calculations two different approaches are investigated for the placement of stirrups. Figure 4.30 a) shows the beam member with stirrups modelled as transverse reinforcement, while in Figure 4.30 b) the structural element is considered with inclined rebars to account for shear.

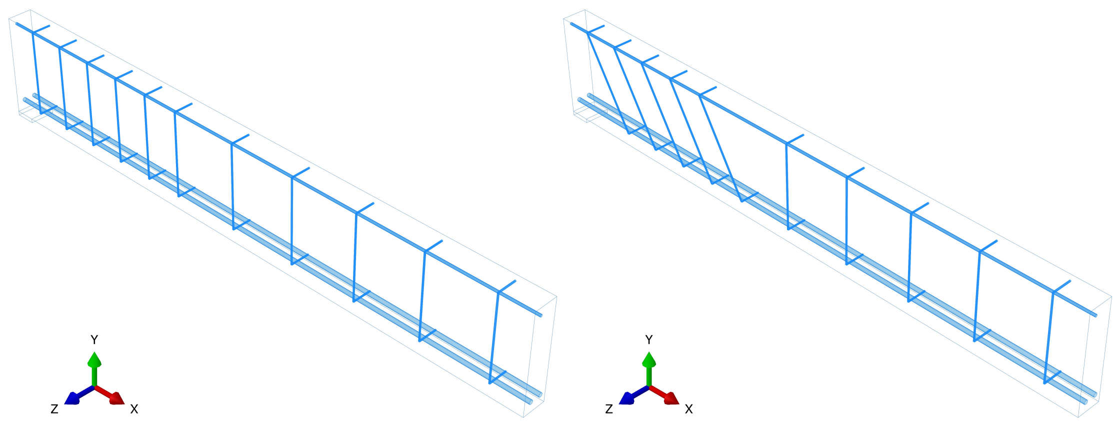

Figure 4.30. Beam with a) transverse reinforcement and b) inclined reinforcement.

In order to see if the vertical stirrups contribute to the main shear resistance of the beam, the reinforcement must be checked for longitudinal tensile stresses in the corresponding bars.

As mentioned in Section 3.4 and visible in Figure 3.9 b) the compressive and tensile stresses change direction closer to the supports. Fortunately, the direction of the stresses can be shown with the aid of ABAQUS and as expected, both the transverse and inclined rebars exhibit tensile stresses, with Figures 4.31 a) and b) emphasising this idea. The transverse reinforcement seems to reach the yielding point while the inclined rebars are just beyond it, having a maximum value of 200 MPa. This is however unexpected due to the fact that a concrete section reinforced for shear, as shown in Figure 4.31 b), should give a safer design in the end, meaning more tensile stress should be present in the inclined bars than in the transverse ones. Moreover, the same trend occurs also for the MC as it is illustrated by Figure 4.32. Even more so, it appears that MC underestimates the actual stresses in the stirrups and as a result it is better to use this model as a crude evaluation only.

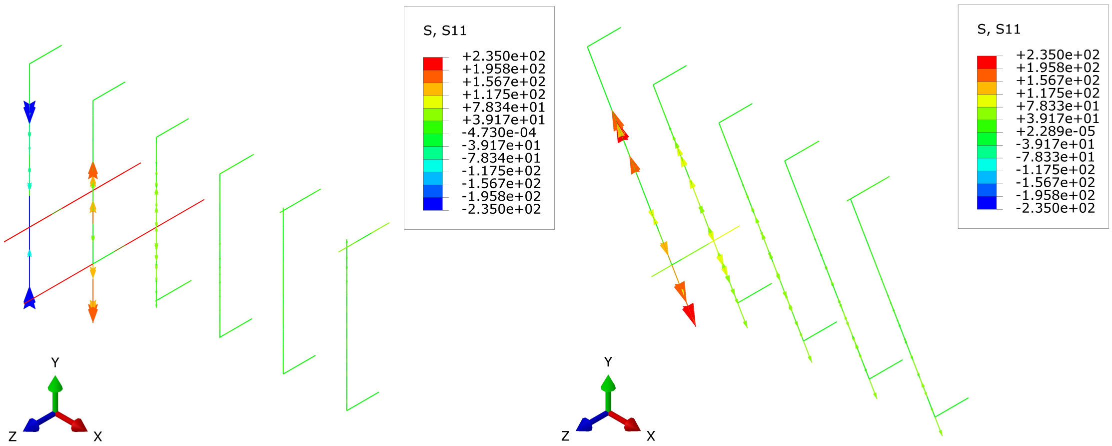

Figure 4.31. Tensile stresses, in CDP model, close to support for a) transverse reinforcement and b) inclined reinforcement.

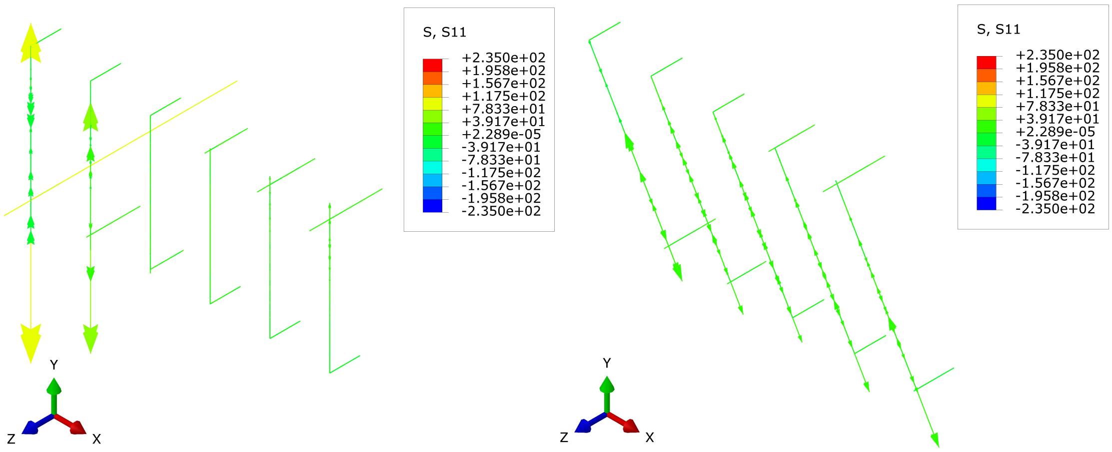

Figure 4.32. Tensile stresses using MC model for a) transverse reinforcement and b) inclined reinforcement.

The difference between transverse and inclined reinforcement is of significance closer to the supports and here it must be stated the implemented design for the steel plates might be unsatisfactory and influence the results. In order to reduce this impact, a point is chosen in the second stirrup from the support for a proper investigation in terms of tensile stresses in the rebars (see Figure 4.33).

It is visible in Figure 4.34 a) that the inclined bars are stressed more and more as the load increases, but the bearing capacity is lower compared to the beam having transverse shear reinforcement. Furthermore, in the concrete body the compressive stresses near the vertical stirrup are reaching slightly higher values. This emphasises that the beam failure could be due to bending and if shear would have been of importance the bearing capacity should be higher for the beam reinforced with inclined rebars.

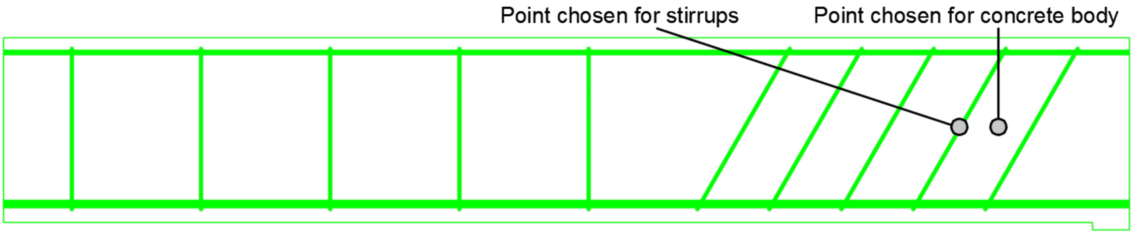

Figure 4.33. Points location for the examination of stresses in both concrete and steel.

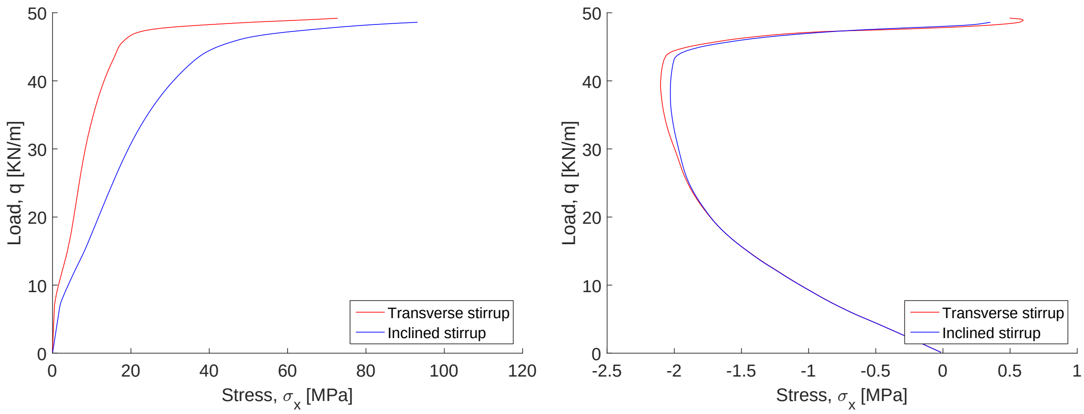

Figure 4.34. Load as a function of: a) Tensile stresses in the shear reinforcement and b) Compressive stresses in the concrete. Displayed results are for the CDP model.

Performed experiments revealed that usually concrete cracks when tensile strain exceeds values in the interval 0.01 to 0.012 [Pascu, 2008]. Thus, an attempt of displaying the cracking regions in the concrete member is visible in Figure 4.35. This is done by limiting such strains to the established interval, resulting in the end with the corresponding areas being removed from the member. With respect to Figure 3.11, it can be stated that most of the cracks are mainly due to flexure, as no combination of flexure-shear cracks or web crushing closer to the support seems to take place. This can be attributed to the fact that damage parameters are not included in the CDP simulations. Hence, the pictured areas are considered to be merely a guess. Furthermore, it must be stressed out that the beam has a length of 6 m and this could underline once more the previously enunciated interpretation that the main failure mechanism is due to bending and actually can be catalogued as pure bending.

Moreover, the presence of stirrups increases by small amount the bearing capacity and a decreased displacement is observed from the normally reinforced concrete beam with longitudinal rebars. These results are given in Table 4.7 and visible in Figures 4.36 a) and b). Due to the small difference between the type of stirrups used, either transverse or inclined, only the transverse results are shown in the figures.

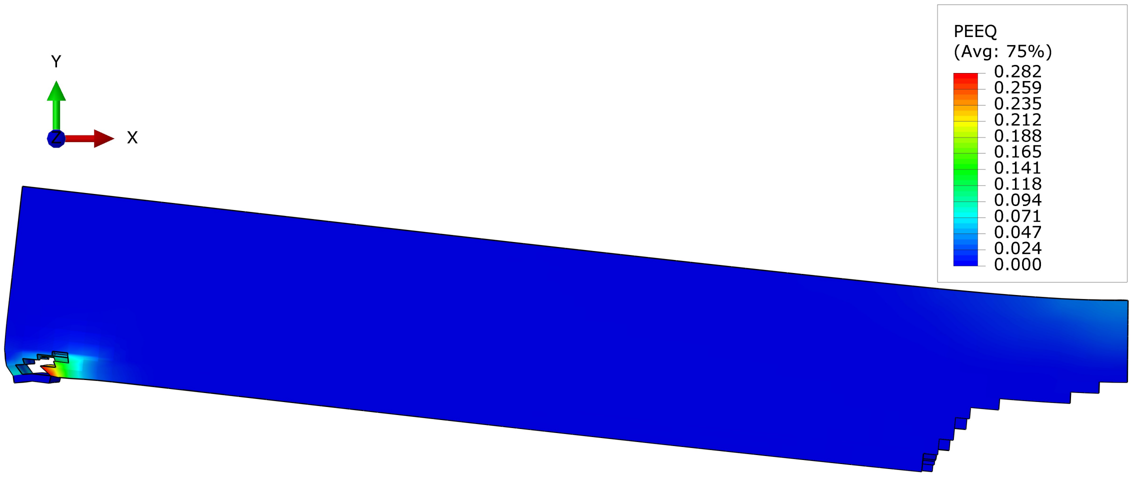

Figure 4.35. Areas where cracks may occur in the concrete beam as predicted by ABAQUS.

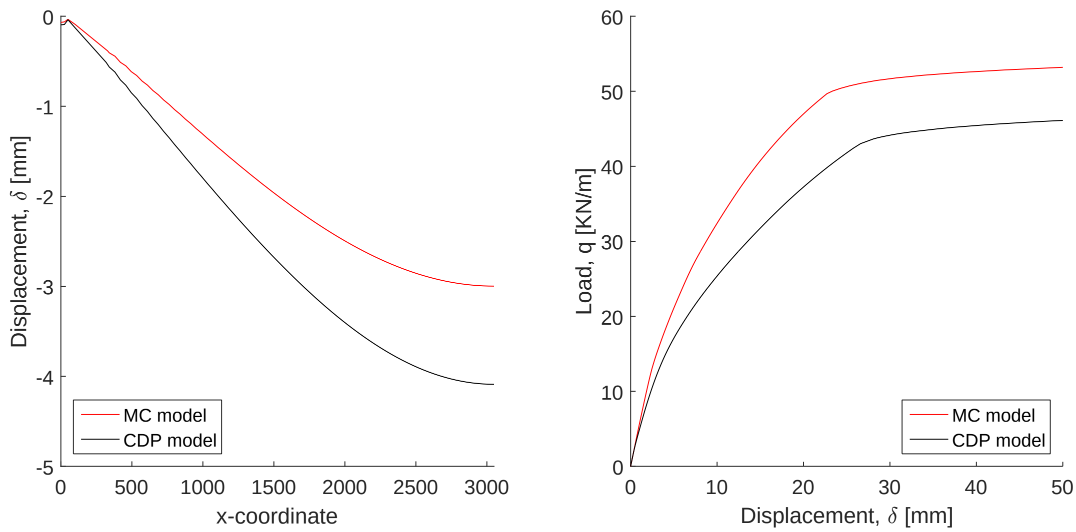

Figure 4.36. MC and CDP results in terms of a) displacement and b) bearing capacity. Shear reinforcement modelled as transverse rebars.

Table 4.7. FE analysis results.

Type of bars	δ [mm]	M_{cap} [KNm]	$q_{cap}\left[\frac{\text{KN}}{\text{m}}\right]$
MC model	SLS	ULS	
Transverse	3.00	243.08	54.02
Inclined	3.00	243.06	54.01
CDP model	SLS	ULS	
Transverse	4.09	219.37	48.75
Inclined	4.09	218.71	48.60

Part II

Discussion and end remarks

Comparison 5

Results obtained from the analytic approach and numerical analysis are compared in this chapter in order to conclude which applied FE technique captures best the concrete response under external loading. The calculations are to be found on [Enclosures-CD, Chapter 5].

Singly reinforced beam

In order to better visualise the results obtained using the two different approaches, either by considering the analytic calculations that follow the regulations imposed by EN1992-1-1 [2014] or involving a FE commercial softwares like ABAQUS, they are plotted against each other as relevant line graphs. Along these lines Figure 5.1 a) shows the displacements obtained for an applied uniform load of 15 KN. It is seen that the analytic results agree more for the SLS case with the values obtained using the MC model, while those achieved with the aid of CDP being much more on the safer side. The difference between MC and CDP can be explained by looking at the slope of the load-displacement curves shown in Figure 5.1 b). In the CDP case compression hardening is taken into account which means that the displacements are actually increasing due to the presence of plastic strains (see also Figure 4.21). Moreover, it is noticeable that up to a load of 7 KN both the MC and CDP follow the same trend which means that ideally a load in that range would have been better for a comparison in term of displacements.

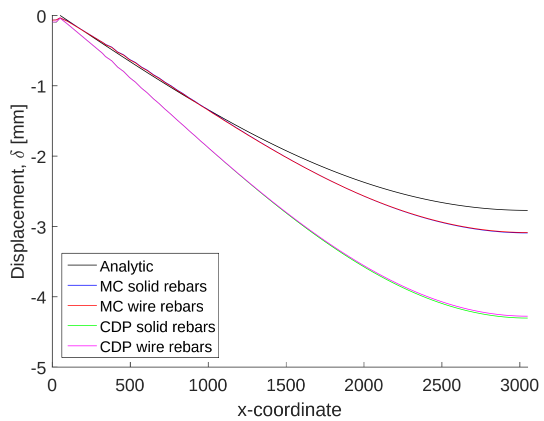

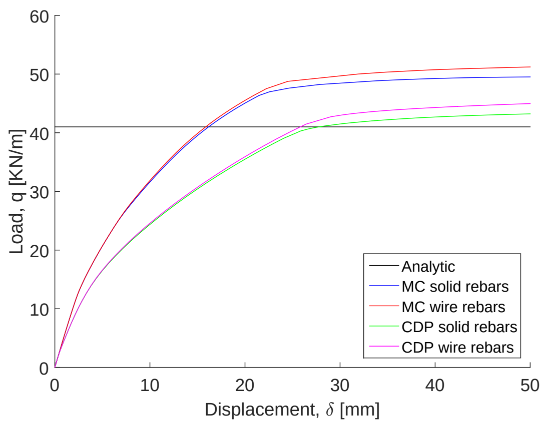

Figure 5.1. Comparison between analytic and FE results in terms of a) displacement and b) bearing capacity.

When considering the ULS scenario it appears that for this case the bearing capacity resulted from the use of CDP model is much more closer to the analytical computed values. This relates back to the involved theory as the equations provided by EN1992-1-1 [2014] and used to determine the bearing capacity include plastic effects. This is not the case when displacements are calculated, as in this project the Euler-Bernoulli beam theory is considered only for linear-elastic response. The difference between analytic and FE results at failure can be attributed to the actual stresses in the concrete. Hence, in Figure 5.2 a) the stresses in the x axis direction are plotted along the height of the beam and it is visible that the current analytic equations does not account for tensile stresses in concrete. So, the extra area which is obtained during FE simulations contribute to the main resistance of the beam and in the end a higher bearing capacity is reached. With respect to the MC model it is seen that the compressive stresses are overestimated even more, thus leading to an even bigger load before failure. Furthermore, the calculated height of the compressed area is much more conservative for the analytic case in contrast to the one resulted from ABAQUS. It is however important to point out that both MC and CDP plasticity predict more or less the same height of concrete in compression and the same tensile stresses.

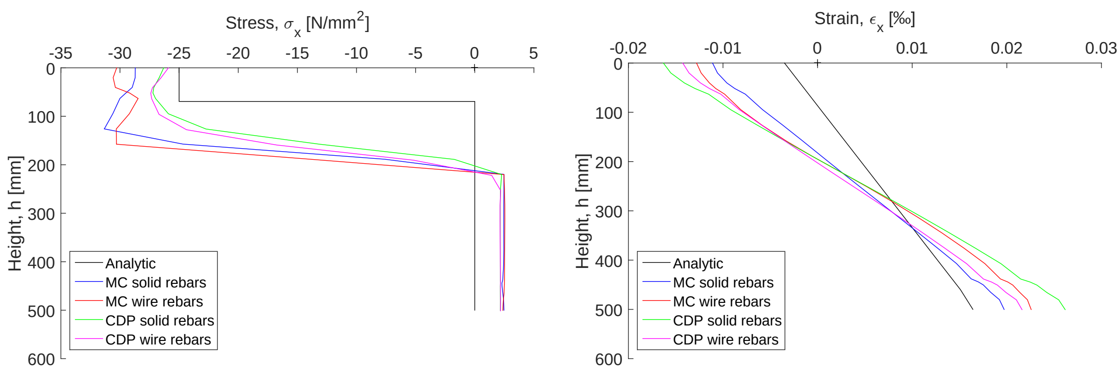

Figure 5.2. Distribution on the height of the beam for different applied methods in case of a) stresses and b) strains.

Figure 5.2 b) show the strain distribution along the height of the section. First and foremost it is essential to underline that the actual strains in concrete do follow a linear trend in some way. [EN1992-1-1, 2014] states a ultimate strain value of 0.0035 for the concrete material which is why the difference appears on the top fibre. By analysing the strains on the bottom fibre it is visible that the analytic and FE strains agree more with each other, but once more the equations provided by Eurocode gives conservative results.

Doubly reinforced beam

More or less the same tendency as for the case of a singly reinforced concrete section is observed once more. What vary are the magnitude of the differences between solid and wire elements used to model the longitudinal reinforcement and which can be seen in Figures 5.3 a) and b) for SLS and ULS respectively. Thus, in this instance they are slightly larger compared to the previous performed analysis.

A rather bizarre and unexpected behaviour is visible in Figure 5.4 b) where the strain distribution for the CDP simulation by using wire elements diverge by quite a margin from the other three carried analyses. This can be attributed to an error which slipped during the reinforcement modelling process or some bad input defined for the longitudinal bars placed in the compressive side.

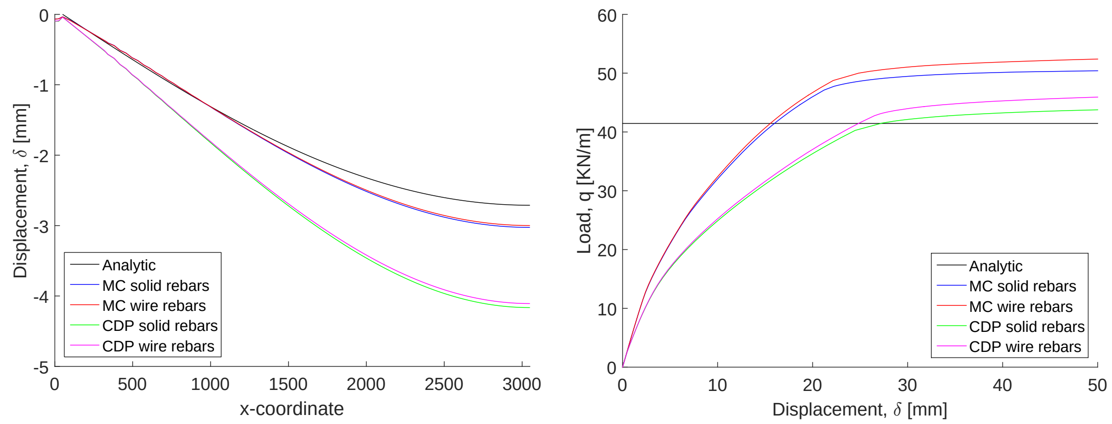

Figure 5.3. Comparison between analytic and FE results in terms of a) displacement and b) bearing capacity.

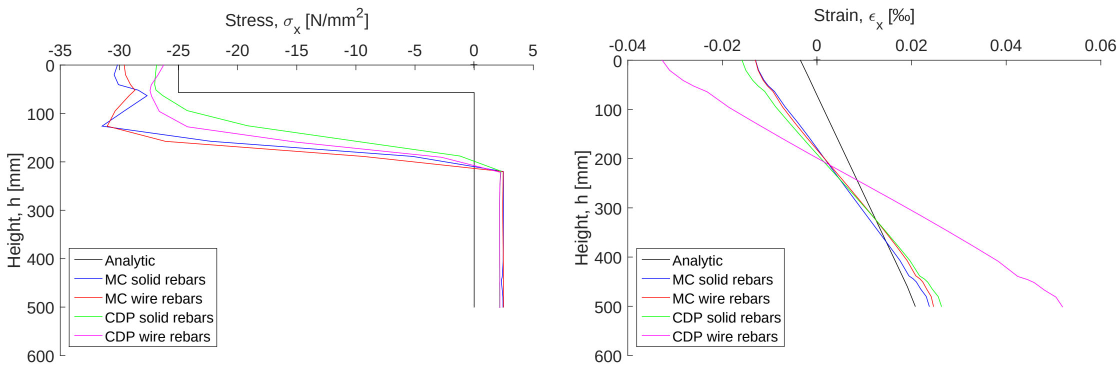

Figure 5.4. Distribution on the height of the beam for different applied methods in case of a) stresses and b) strains.

Shear reinforcement

Since the flexural rigidity of the beam with stirrups is not computed, results are not available for the SLS case using the analytic procedure, thus a direct comparison can be established in terms of bearing capacity for ULS only. Nevertheless, usually stirrups have no significant effect in terms of deformation and they are provided for resistance reasons only. As stated in Section 4.4 the reinforcement is modelled using wire elements, so the results are presented for this case only.

In Figure 5.5 it is visible that a relatively high increase in bearing capacity is obtained from the transverse to the inclined stirrups when using the current available equations. It must be stressed out that an angle of 60° has been used for the inclination of the bars in the analytic calculations. On the other hand, the difference between transverse and inclined reinforcement for both MC and CDP models is almost inexistent and this as explained previously is due to the nature of failure in the beam. As noticed for the singly and doubly reinforced concrete sections with longitudinal rebars, the CDP supply results closer to the analytical ones also when shear reinforcement is involved.

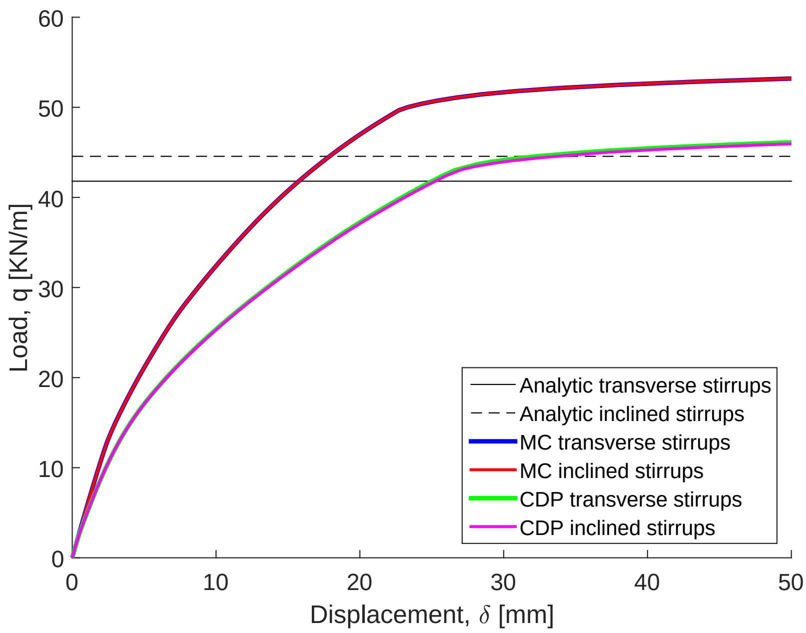

Figure 5.5. Comparison with respect to bearing capacity of the beam. Reinforcement modelled as wire elements.

Reinforced concrete sections

Figure 5.6 a) and b) illustrate that each time steel is adequately placed in relevant tensile regions of the concrete beam the displacement decreases and the resistance increases. Hence, this is a quick way of demonstrating how important the combination of steel and concrete is when designing structures made of reinforced concrete.

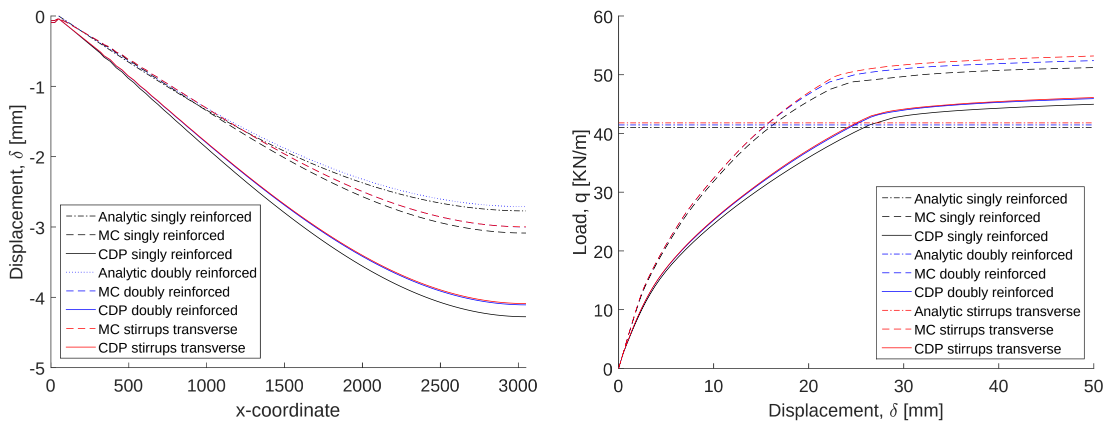

Figure 5.6. Comparison between involved sections in terms of a) displacement and b) bearing capacity.

Conclusion 6

Nowadays buildings are getting larger and taller and the heterogeneous reinforced concrete material seems to still keep pace with the new obstacles.

Available methods and design formulae possess different assumptions on the actual behaviour of concrete. The idealized stress-strain distribution, along the height of the beam cross-section, from the involved analytic procedure predict conservative results in terms of bearing capacity, stresses, strains and compressed area of concrete. Moreover, the use of Euler-Bernoulli beam theory for elastic problems underestimates the actual displacement even in case of loads of small magnitude, and as such an adaptation to elasto-plasticity would be better.

For a reinforced concrete beam a range of factors can influence its failure mechanism. In case of a simply-supported beam subjected to uniformly distributed load and having greater spans, investigations revealed that the main failure is due to flexure-cracks, which seems likely as shear force effects are of much more importance in case of concentrated loads and shorter beams.

Different types of reinforcement can be attributed to strengthen the member. For the analysed structural element, longitudinal reinforcement placed on the tensile fibre has the largest influence on the bearing capacity, while rebars placed on the compressive part or in order to account for shear also contribute by small amount to the main resistance.

From the treated constitutive models, Concrete Damage Plasticity seems to capture the response of concrete best, while if the case implies stress reversals can be taken into account. Compression hardening laws can be implemented and the performed finite element studies showed that the bearing capacity and stress-strain distributions agrees well to the ones calculated by means of analytic calculations. Furthermore, if experiments are conducted beforehand certain damage parameters can be used as input data to accurately predict the cracking patterns in the beam. Nevertheless, proper performed simulations demonstrated that concentrations of plastic strains end up in accurately predicted regions and as a result areas where cracks might occur can still be found. With respect to the MC model, performed studies showed that the bearing capacity might end up being overestimated if the tensile stress is not limited to the actual tensile strength of concrete. Moreover, since implementation of hardening laws are rather difficult to apply the displacement is underestimated. However, the prediction of stresses of strains agree to those obtained by the use of a more reliable concrete material model.

A further study of the accurate representation of cracking patterns with the aid of numerical model should to be done. Furthermore, currently available constitutive models gives much better representation of the loading problems than the standards currently used.

Bibliography

Abaqus, 2016. Abaqus. *Abaqus 6.12 Documentation Manual*, 2016. Downloaded: 12-01-2016.

ACI318M, 1995. ACI318M. *ACI 318: Building Code Requirements for Reinforced Concrete*, 1995.

Bruno Massicotte and MacGregor, 1990. Alaa E. Elwi Bruno Massicotte and James G. MacGregor. *A Study Of Combined Bending And Axial Load In Reinforced Concrete Members*. 116:11(3039). American Society of Civil Engineers, 1990.

Det Norske Veritas, 1992. Det Norske Veritas. *Det Norske Veritas - Foundations - Classification notes NO. 30.4*. 1992.

EN1992-1-1, 2014. EN1992-1-1. *Eurocode 2: Design of concrete structures - Part 1-1 : General rules and rules for buildings*, 2014.

Enclosures-CD. Enclosures-CD. *CD with enclosures belonging to Laurentiu-Fabian Bitiusca*.

Hognestad, 1951. Eivind Hognestad. *A Study Of Combined Bending And Axial Load In Reinforced Concrete Members*. Buletin Series No. 899. University of Illinois, Urbana, 1951.

IS456, 2000. IS456. *IS 456: Plain and Reinforced Concrete Code of Practice*, 2000.

Jeeho Lee, 1998. Gregory L. Fenves Jeeho Lee. *Plastic-Damage Model for Cyclic Loading of Concrete Structures*. Journal of Engineering Mechanics, 124, 892–900, 1998.

Lublinier, 1989. J. Lublinier. *A Plastic Damage Model for Concrete*. International Journal of Solids and Structures, 25, 299–329, 1989.

MacGregor and Wight, 2012. James MacGregor and James Wight. *Reinforced concrete - Mechanics and design*. Pearson Education, 2012.

Moghrabi, 2006. Rabih Moghrabi. *Burj Dubai Unveiled*. URL: `https://www.theguardian.com/artanddesign/gallery/2010/jan/04/burj-dubai-unveiled#img-6`, 2006. Downloaded: 11-07-2016.

Niels Saabye Ottosen, 2005. Matti Ristinmaa Niels Saabye Ottosen. *The Mechanics of Constitutive Modelling*. Elsevier, 2005.

NSCP, 2010. NSCP. *National Structural Code of Philippines, 6th Edition*, 2010.

Pascu, 2008. Radu Pascu. *Comportarea si calculul elementelor din beton armat [Behaviour and computation of reinforced concrete elements]*. Technical University of Civil Engineering Bucharest, 2008.

Vasshaug, 2013. Håvard Vasshaug. *Structural rebars in beam*. URL: `https://vasshaug.net/gallery/`, 2013. Downloaded: 11-07-2016.

Y. Fujita, 1994. R. Ishimaru Y. Fujita. *Study on internal friction angle and tensile strength of plain concrete*, 1994.

Stress-strain distribution under SLS A

A.1 Singly reinforced beam

In the past the design of reinforced concrete cross-sections were based on the elastic theory, but nowadays the ultimate limit method has outperformed the previous type. However, with respect to the displacement calculations, for ensuring that the assumption of linear-elastic behaviour is tolerable under a load of 15 KN, the Working Stress Design (WSD), commonly known as Alternate Design Method (ASD), is used [ACI318M, 1995]. This method has its basis on the theory of elasticity where the stress-strain distribution seen in Figure A.1 obeys Hooke's Law. Thus, some assumptions are made and they are listed as follow:

- Sections remain plane before and after bending.
- Tensile stress is carried by the steel reinforcement, while concrete has contribution only to the compressed zone.
- Stress-strain relationship of both materials is a straight line.
- The no-slip condition is applied, which means the two materials are perfectly bound to one another.

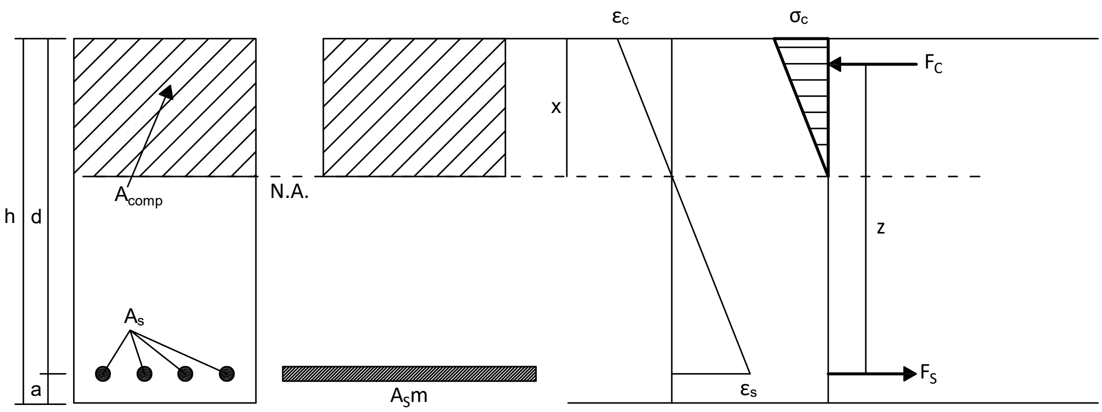

Figure A.1. Stress-strain distribution by ASD method.

In order to solve this problem an equivalent area of concrete is assumed instead of the one of real steel. To do so, the modular ratio coefficient m is considered and solved by Equation (A.1) [Pascu, 2008].

$$m = \frac{E_s}{E_{cm}} \tag{A.1}$$

Furthermore, permissible stresses in SLS for the two materials are involved instead of their ultimate values. While ACI318M [1995] and NSCP [2010] suggests a value of σ_c^{perm} equal to $0.45 f_{ck}$, IS456 [2000] indicates that this is 8.5 MPa for a concrete class C 25 which is actually close to $0.35 f_{ck}$. For steel in most codes σ_s^{perm} is given as 140 MPa for a class S 350 or lower. Thus, the considered values are $0.40 f_{ck}$ for concrete and 140 MPa for steel.

The height of the compressed area, x, is calculated by the method of equilibrium given in Equation (A.2) from which the absolute value of x is taken into account.

$$\frac{bx^2}{2} + mA_s x - mA_s d = 0 \tag{A.2}$$

where

d	design height of the cross-section
A_s	total area of steel

It is imposed that the value of x to be smaller than x_b which means is better to use an amount of steel (or a steel class) in the beam less than that at a balance failure (see Figure 3.4 b)). By doing so, the actual stress in steel reaches the σ_s^{perm} while the stress in concrete is less than σ_c^{perm}.

Next the resisting moments in the beam when the stress reaches σ_c^{perm} and σ_s^{perm} are calculated by Equation (A.3) from which according to the elastic theory the minimum value of the two should be taken into account.

$$\begin{aligned} M_r &= \min\left(M_{rc}, M_{rs}\right) \\ M_{rc} &= F_c z = \frac{\sigma_c^{perm}}{2} bxd \left(x - \frac{d}{3}\right) \\ M_{rs} &= F_s z = \sigma_s^{perm} A_s d \left(x - \frac{d}{3}\right) \end{aligned} \tag{A.3}$$

where

M_{rc}	resisting moment calculated corresponding to concrete area
M_{rs}	resisting moment calculated corresponding to steel area
z	the arm of the force

From the moment equilibrium equation of a simply-supported beam the bending moment can be calculated at the mid-span of the beam. Thus, the solution of Equation (A.4) after imposing the value of M_r is the maximum load in SLS.

$$M_{mid} = \frac{ql^2}{8} \Rightarrow q_{SLS} = \frac{8M_r}{l^2} \tag{A.4}$$

where

q_{SLS}	maximum load in SLS

The displacement at the mid-span is introduced already in Section 3.1.1 with the Equation (3.4). Thus, q_{SLS} is substituted and the allowed displacement according to the analytical calculations is afterwards found. The results for the SLS case are found in Table A.1

Table A.1. Analytic results for SLS.

M_r [KNm]	$q_{SLS}\left[\frac{\text{KN}}{\text{m}}\right]$	δ [mm]	ε_s [-]	ε_c [-]	x [mm]
72.41	16.09	2.97	0.00067	0.00031	145.29

A.2 Doubly-reinforced beam

Same ASD method as implied for the singly reinforced cross-section beam is performed for this case. The only difference is the influence of the new considered steel bars which as shown in Figure A.2 are placed in the compressed area.

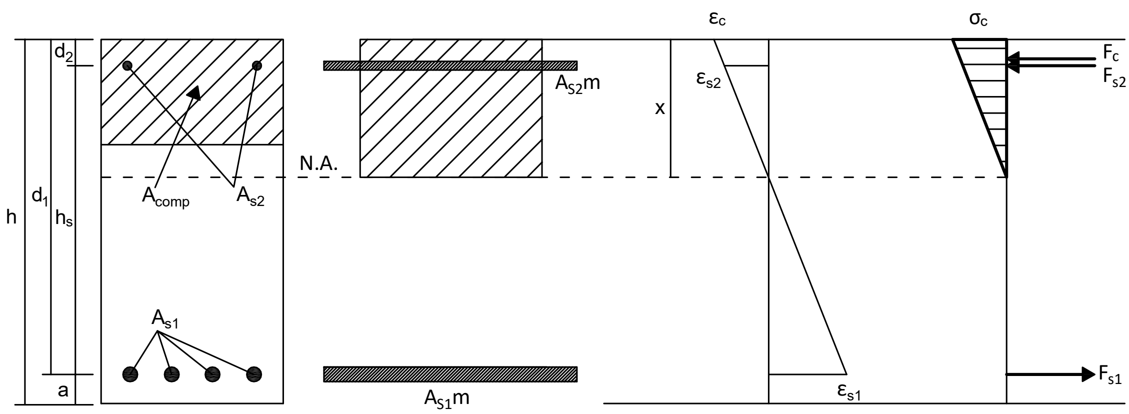

Figure A.2. Stress-strain distribution by ASD method.

The position of neutral axis is given by Equation (A.5) and is calculated by considering moments of area about the neutral axis. The same yielding criterion as specified previously in Equation (3.8) must be checked in order to ensure that steel in the tensioned side reaches yielding before failure of the concrete. Moreover, the absolute value of x is the considered height in compression.

$$\frac{bx^2}{2} + (m-1)\,n_{h2}A_{s2}\,(x-d_2) - mn_{h1}A_{s1}\,(d_1-x) = 0 \tag{A.5}$$

where

A_{s1}, A_{s2}	area of the tensioned and compressed steel bar respectively
d_1, d_2	design heights of the cross-section corresponding to case a) and b)

However, another criterion, as specified in Equation (A.6), is imposed for top reinforcement of the beam. This is more or less just a verification to see if the steel bars placed in this location reach yielding or not as it is not necessary a requirement in doing so. By not reaching yielding is just an issue from the economical point of view as an over-reinforced beam will be obtained but the rebars placed in the tensile zone will carry over the stress.

$$\frac{x_{min}}{d_2 - x_{min}} = \frac{\varepsilon_c}{\varepsilon_s} \Rightarrow x_{min} = d_2\frac{\varepsilon_c}{\varepsilon_c - \varepsilon_s} \tag{A.6}$$

where

A_{s1}, A_{s2}	area of the tensioned and compressed steel bar respectively
d_1, d_2	design heights of the cross-section corresponding to case a) and b)

Thus, the resisting moment, M_r, is calculated accordingly which means that the imposed criteria must be met and steel will yield prior to failure of concrete. The Equation (A.7) show the implied iteration procedure.

$$\begin{cases} M_r = \min\left(M_{rc}, M_{rst}\right) \\ M_{rc} = \dfrac{bx\sigma_c^{perm}}{2} z + (m-1)\, n_{h2} A_{s2} \sigma_c^{perm} h_s \quad , \quad x_{min} \leq x \leq x_b \\ M_{rst} = n_{h1} A_{s1} \sigma_s^{perm} h_s \end{cases} \tag{A.7}$$

$$M_r = M_{rst} \quad , \quad x < x_{min} \tag{A.8}$$

where

M_{rc}	resisting moment calculated corresponding to concrete area [KNm]
M_{rst}	resisting moment calculated corresponding to steel area in tension [KNm]

After M_r is established, the corresponding load, q_{SLS} is calculated in the same way as for the singly-reinforced concrete beam. Afterwards, the displacement is found with the aid of Equation (3.4) given by Bernoulli's beam theory. The results for a concrete beam reinforced with both compressed and tensioned bars are visible in Table A.2.

Table A.2. Analytic results for SLS.

M_{cap} [KNm]	$q_{cap}\left[\frac{\text{KN}}{\text{m}}\right]$	δ [mm]	ε_{s1} [-]	ε_{s2} [-]	ε_c	x [mm]
74.59	16.58	3.00	0.00068	0.00023	0.00031	142.21

Numerical investigations B

B.1 Observations and analyses

Generally the range of the Poisson's ratio for sand is between 0.125 - 0.30 and for clay between 0.20 - 0.40 [Det Norske Veritas, 1992]. Moreover for concrete, these values are taken in between 0.10 and 0.20 and according to EN1992-1-1 [2014] the best is to consider it equal to 0.20. Empirical relationship between the strength and deformation parameters has been elaborated for the case of sands by Det Norske Veritas [1992] and since concrete appears to have a Poisson ratio in the same interval, the equation Equation (B.1) is used as an explanation for the numerical results obtained by using the MC model.

$$\nu = \frac{1 - \sin\phi}{2 - \sin\phi} \tag{B.1}$$

where

ν	Poisson's Ratio
ϕ	friction angle of the material

In order to examine the way in which the beam deflects, contour plots illustrating the displacements are shown in Figure B.1 for the MC model and Figure B.2 for CDP model.

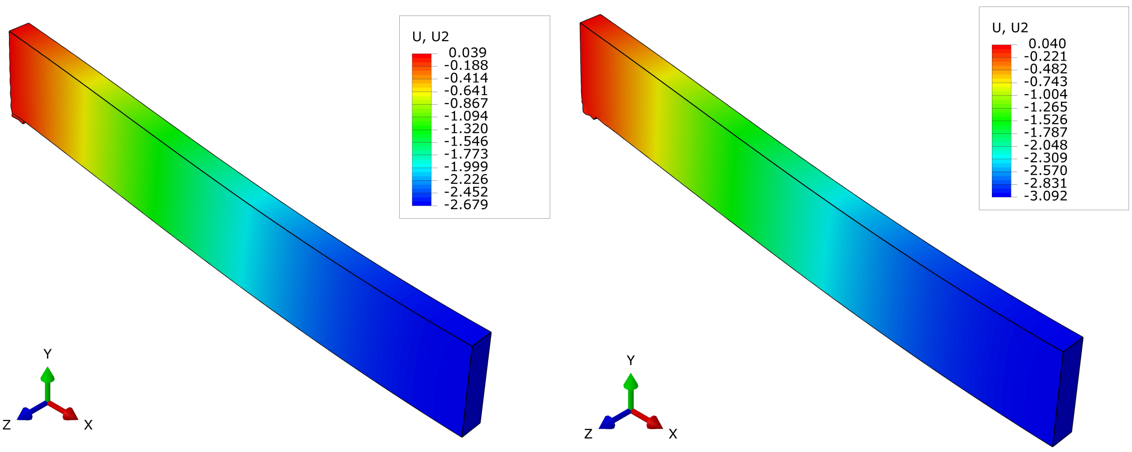

Figure B.1. Beam displacement with a) friction angle of 37 ° and b) friction angle of 55 °. Reinforcement modelled as wire elements.

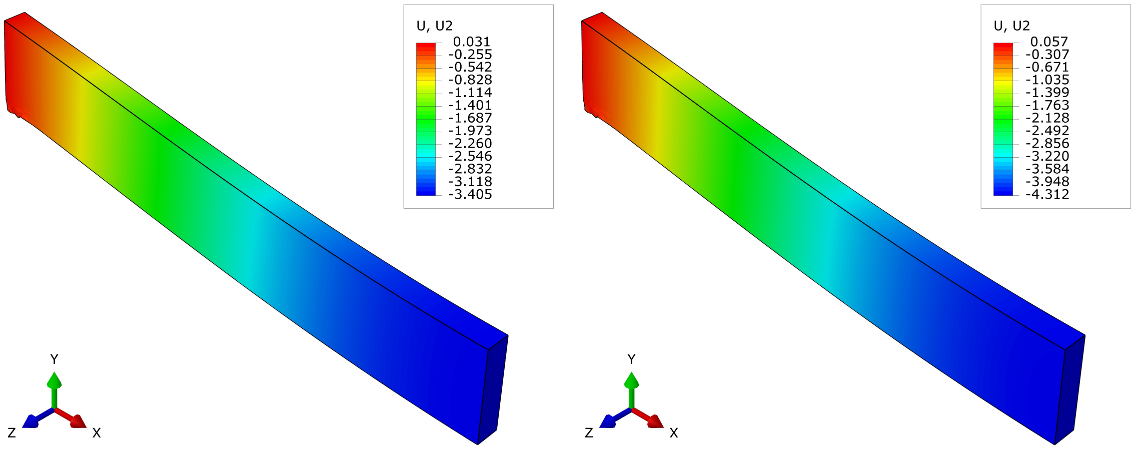

Figure B.2. Displacement in a) idealised behaviour model and b) in hardening behaviour model. Reinforcement modelled as solid elements.

There are different types of non-linearity that could arise during loading. **Material** non-linearity can occur due to changes in the material properties while the analysis take place. This can involve cases such as plasticity or visco-plasticity. Secondly there is **contact** non-linearity which means which are due to changes in the boundary conditions during analysis. Lastly, there is **geometric** non-linearity which account for geometry changes like large displacement analysis.

In ABAQUS there is a possibility of accounting for non-linear geometry analysis. Thus, if the geometry of your object changes due large displacements and/or rotation during the simulation, the initial linear stiffness matrix must be updated in order to distinguish between the reference undeformed model and the current deformed one. A quick investigation is performed to see by what margin the results are diverging while having the option On or OFF (see Figure B.3).

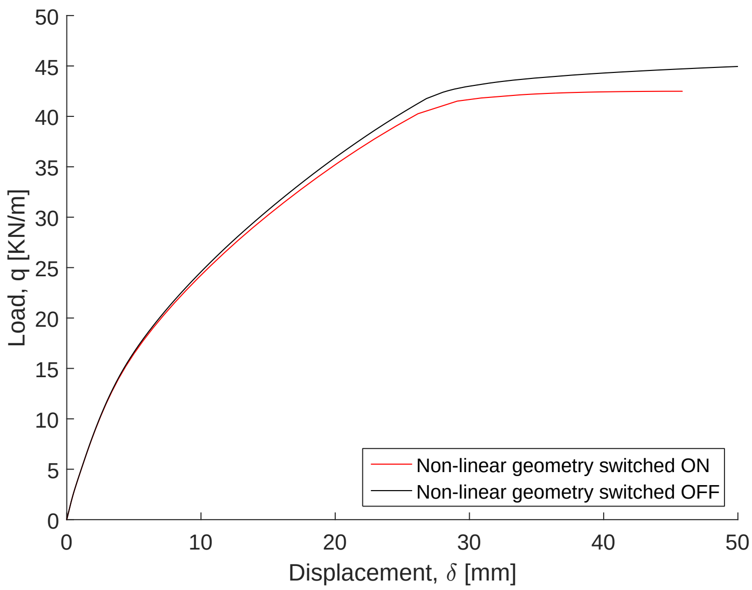

Figure B.3. Sensitivity analysis in terms of bearing capacity to **nlgeom**. Reinforcement modelled as wire elements.

In the numerical part of the project the meshing of the beam is done by using C3D8R elements having only one integration point. More integration points indicate more accurate results if the chosen mesh is coarse. The difference between elements having one or four integrations points is analysed and the results are shown in Figure B.4.

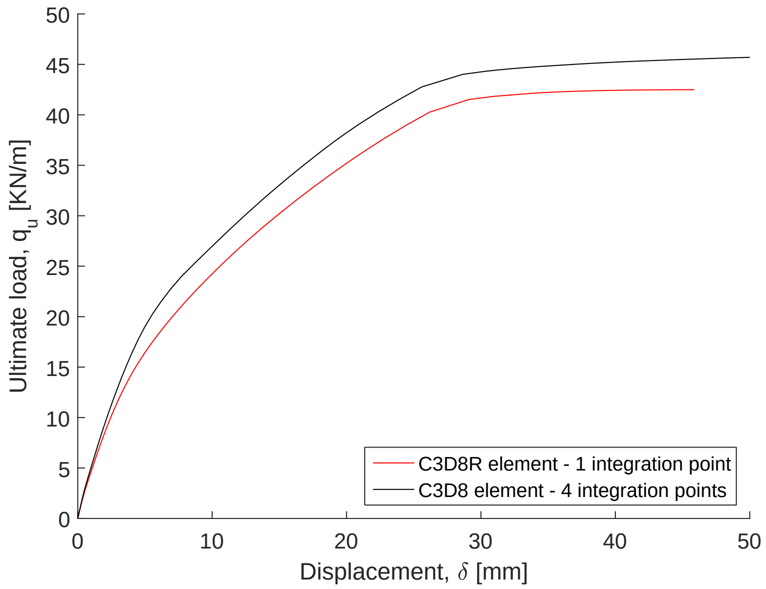

Figure B.4. Sensitivity analysis in terms of bearing capacity to the number of integration points. **nlgeom** option ON. Reinforcement modelled as wire elements.

B.2 Singly reinforced beam

For the SLS casee the load is chosen such that it is assumed the reinforced concrete beam is still under linear-elastic response. Hence, to investigate displacements and to assure to a certain degree that the assumption is acceptable, a rather simple way is to check for plastic strains under the considered load. Figure B.5 illustrate no such strains and as a consequence the material is assumed to behave elastically.

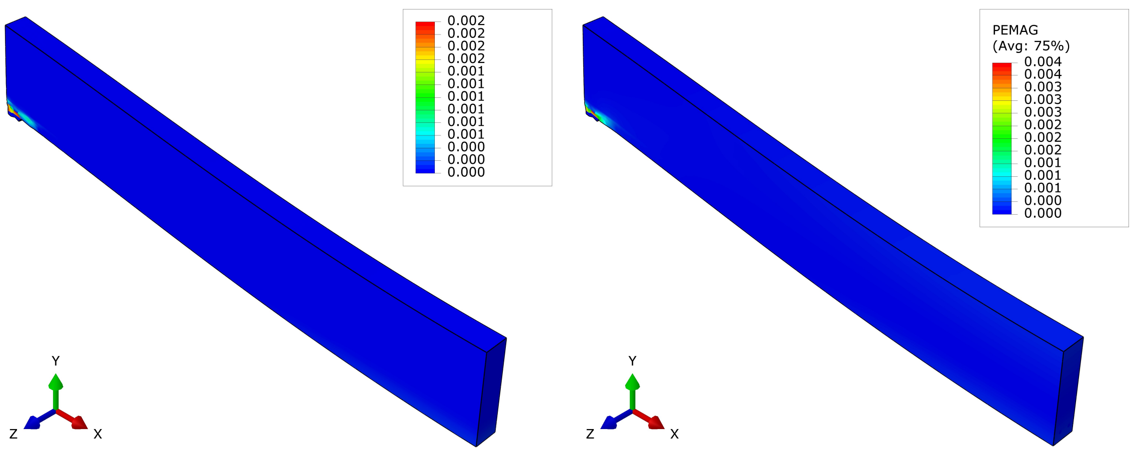

Figure B.5. Check for plastic strains for SLS case in a) MC model and b) CDP model. Reinforcement modelled as wire elements.

The difference in displacement with respect to the approach made in the modelling process of reinforcement, in both MC and CDP constitutive models, is shown by Figures B.6 and B.7. This difference is almost insignificant and concludes that both wire and solid rebars can be used, with the earlier necessary in order to account for more complex reinforcement geometries.

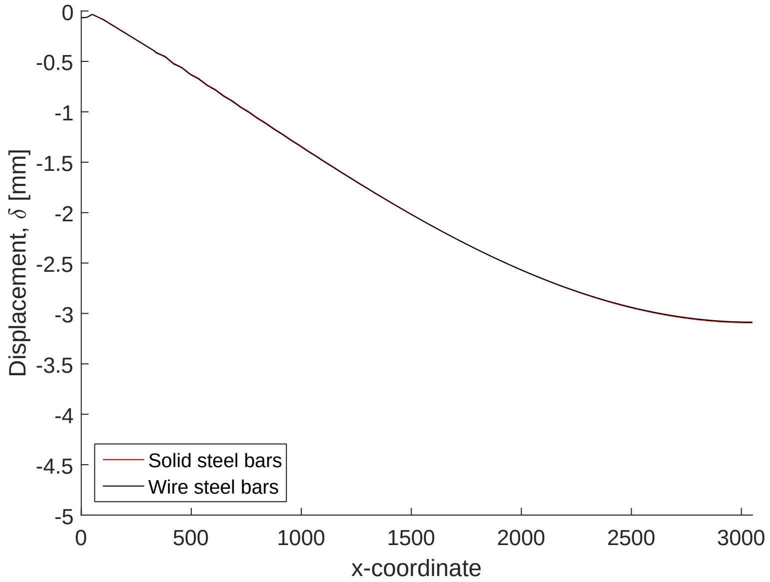

Figure B.6. Beam displacement over length for MC model using solid and wire rebars.

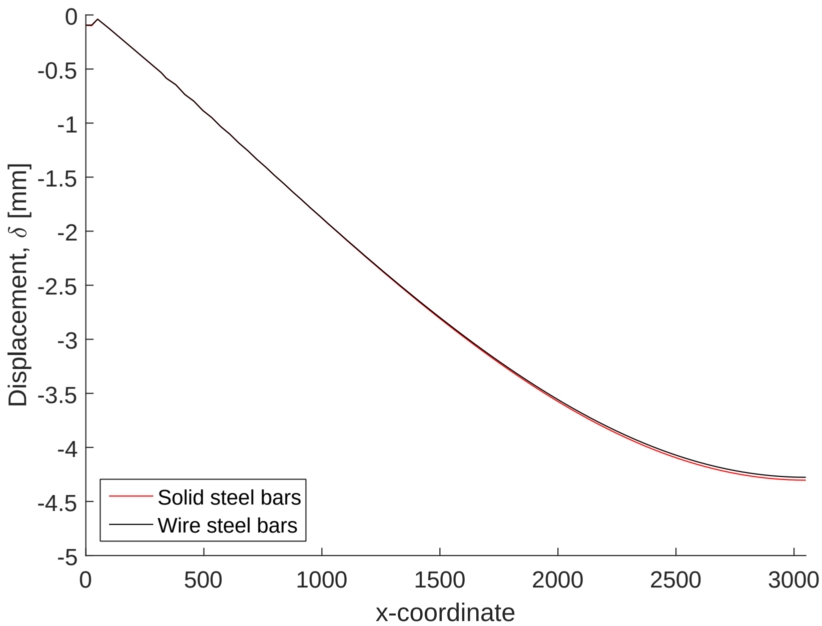

Figure B.7. Beam displacement over length for CDP model using solid and wire rebars.

B.3 Doubly reinforced beam

The contour plots of the plastic strains are shown in Figure B.8, while the obtained displacements are visible in Figures B.9 and B.10.

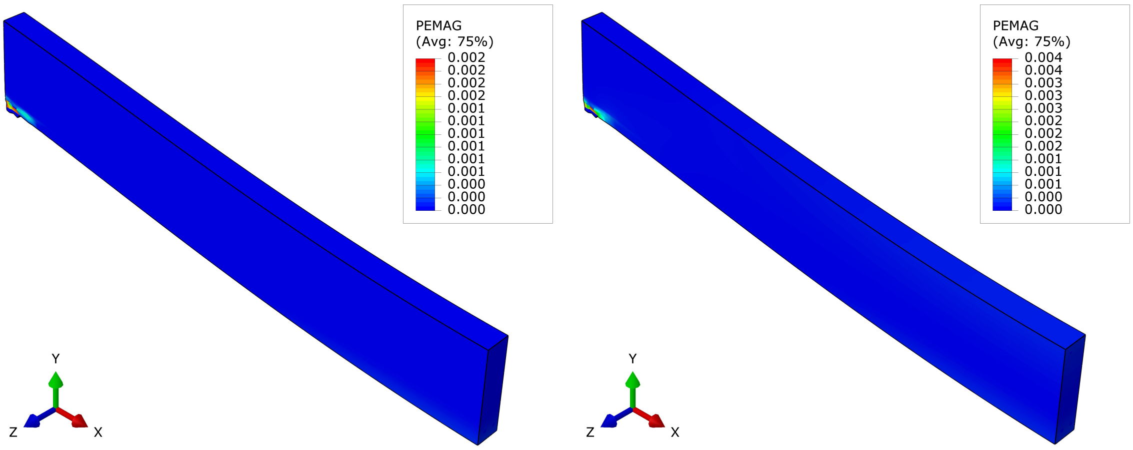

Figure B.8. Check for plastic strains for SLS case in a) MC model and b) CDP model. Reinforcement modelled as wire elements.

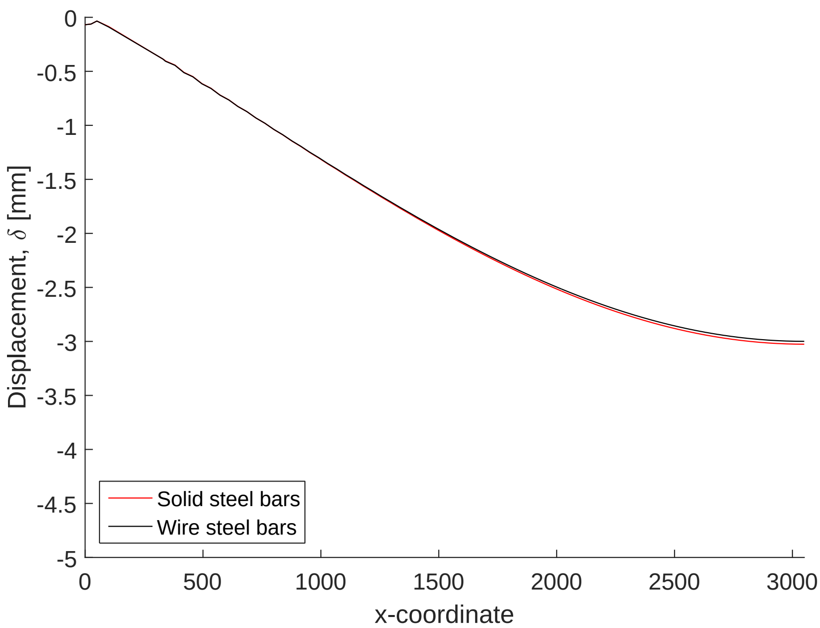

Figure B.9. Beam displacement over length for MC model using solid and wire rebars.

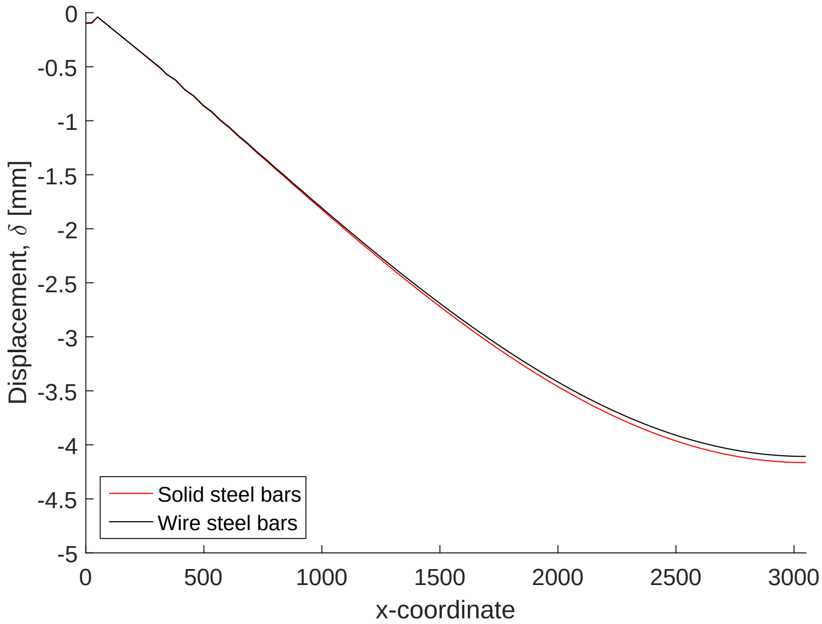

Figure B.10. Beam displacement over length for CDP model using solid and wire rebars.